AGU PUBLICATIONS

JGR

Journal of Geophysical Research: Oceans

RESEARCH ARTICLE

10.1002/2014JC010619

# Hydrographic variability in the St. Helena Bay region of the southern Benguela ecosystem

**T. Lamont[1,2], L. Hutchings[2], M. A. van den Berg[1], W. S. Goschen[3,4], and R. G. Barlow[2,5]**

[1]Oceans and Coastal Research, Department of Environmental Affairs, Cape Town, South Africa, [2]Marine Research Institute, Department of Oceanography, University of Cape Town, Cape Town, South Africa, [3]South African Environmental Observation Network, SAEON Egagasini Node, Cape Town, South Africa, [4]Institute for Coastal and Marine Research, Nelson Mandela Metropolitan University, Port Elizabeth, South Africa, [5]Bayworld Centre for Research and Education, Cape Town, South Africa

**Key Points:**
- Seasonal variation in cross-shelf distribution of water masses
- Zonation of surface waters by the oceanic and bifurcated shelf-break fronts
- A permanent Low Oxygen Water (LOW) reservoir occurs in St. Helena Bay

**Correspondence to:**
T. Lamont,
tarron.lamont@gmail.com

**Citation:**
Lamont, T., L. Hutchings, M. A. van den Berg, W. S. Goschen, and R. G. Barlow (2015), Hydrographic variability in the St. Helena Bay region of the southern Benguela ecosystem, *J. Geophys. Res. Oceans*, *120*, 2920–2944, doi:10.1002/2014JC010619.

Received 3 DEC 2014
Accepted 21 MAR 2015
Accepted article online 4 MAR 2015
Published online 18 APR 2015

**Abstract** Cross-shelf distributions of temperature, salinity, water masses, and dissolved oxygen in St. Helena Bay revealed substantial vertical and seasonal variations. In the surface layers, nearshore and offshore temperature and salinity patterns differed, with bay-scale variability linked to upwelling dynamics and coastal processes, while the offshore region was influenced by solar insolation. Spectral analysis revealed that an annual signal prevailed at most stations, and corroborated contrasting patterns between the offshore and nearshore regions, with phase differences suggesting shoreward propagation of the offshore temperature signal. The shelf was dominated by Modified Upwelled Water (MUW) and Subantarctic Mode Water (SAMW), which comprised the primary source of upwelled water. Clear zonation of MUW was evident across the shelf, resulting from seasonal variations in locations of the oceanic and bifurcated shelf-break fronts. Dynamics within St. Helena Bay consistently differed from those further offshore, due to the influences of the shelf-break front, Cape Columbine upwelling plume, and cyclonic recirculation, which appeared to be associated with an intraannual signal with a periodicity of 3–4 months. Persistent hypoxia in the bottom waters suggested the occurrence of a permanent reservoir of Low Oxygen Water (LOW). Seasonal shoreward and offshore expansion of LOW occurred throughout the upwelling season, with maximum extent reached during summer and autumn, due to the coupled effects of advection and local phytoplankton decay. While wind mixing ventilated the water column at nearshore stations in winter, and the onset of upwelling during spring introduced oxygen-richer water from further offshore, hypoxia persisted in the center of the Bay.

## 1. Introduction

The Benguela Current system is composed of an offshore flow, which forms the eastern limb of the South Atlantic subtropical gyre, and a coastal branch, dominated by upwelling and modulated by local weather processes [*Hardman-Mountford et al*., 2003]. Perennial upwelling at Lüderitz (27°S) comprises an environmental barrier that essentially divides the Benguela into the northern and southern subsystems [*Duncombe Rae*, 2005; *Lett et al*., 2007]. Within the southern Benguela ecosystem, St. Helena Bay (32°S) is the largest embayment on the west coast of South Africa and is an important region for pelagic fish, hake, and rock lobster [*Cockcroft*, 2001; *Cockcroft et al*., 2008; *Fairweather et al*., 2006; *Hutchings et al*., 2012; *Payne and Punt*, 1995; *van der Lingen et al*., 2006]. It is a well-known retention area and has been identified as a region of significantly elevated phytoplankton and zooplankton biomass [*Demarcq et al*., 2007; *Huggett et al*., 2009; *Lett et al*., 2006; *Weeks et al*., 2006]. Comprehensive reviews of the major features of the ecosystem have been provided by *Hutchings et al*. [2009b] and *Shannon et al*. [2006]. The oceanography of the southern Benguela is governed primarily by the interaction of four factors, i.e., equatorward wind stress, mesoscale atmospheric perturbations, topography, and the influence of the Agulhas Current system.

Winds over the southern Benguela are controlled by the atmospheric anticyclone located over the central South Atlantic ocean which drives south-easterly winds along the South African west coast, by the pressure field over the subcontinent, and by eastward traveling midlatitude cyclones south of the continent, which result in periodic weakening or abatement of south-easterly winds along the coast [*Nelson and Hutchings*, 1983]. Seasonal upwelling occurs in the region, with maxima coinciding with peaks in south-easterly trade

winds during spring and summer, while minimum upwelling is associated with prevailing westerly winds in winter [*Shannon*, 1985; *Shannon and Nelson*, 1996]. Upwelling cells are located in regions of cyclonic wind stress curl and, in most cases, are associated with a change in coastline orientation [*Shannon and Nelson*, 1996]. Where the continental shelf is narrow, upwelling tends to be limited to a narrow band along the coast, while in regions where the continental shelf is wide, upwelling extends as far as the shelf edge, with pronounced uplift over the continental slope [*Shannon and Nelson*, 1996]. The characteristics of the major upwelling cells have been described by various authors, including *Nelson and Hutchings* [1983], *Shannon* [1985], and *Lutjeharms and Meeuwis* [1987].

The Agulhas Current retroflects south of Cape Town, shedding Agulhas rings and filaments, which generally move in a north-westerly direction [*Lutjeharms*, 2006]. These rings and filaments have been shown to occasionally interact with the upwelling system and influence the biology on the shelf [*Duncombe Rae et al*., 1992a, 1992b]. Increased westerly winds over the Agulhas Bank appear to correspond to major intrusions of Agulhas Current water into the Southern Benguela [*Hardman-Mountford et al*., 2003]. The intrusion of Agulhas Current water during the winter of 1986 penetrated as far north as Lüderitz and seems to have resulted from anomalies in the distribution of wind stress over the Indian Ocean and the Agulhas Retroflection region [*Shannon and Agenbag*, 1990; *Shannon et al*., 1990]. Similar intrusions of Agulhas Current water between 1957 and 1964 and during the summer of 1992–1993 and June 1994 have been suggested by *Shannon and Nelson* [1996]. During ring spawning at the Agulhas Retroflection, cold subantarctic surface water has been observed to penetrate into the South Atlantic, in the form of filaments extending as far north as 33°S [*Shannon et al*., 1989, 1990]. The shelf-edge front is enhanced off the peninsula south of Cape Town during summer due to the intense upwelling of cold water inshore and the advection of warm Agulhas Current and Agulhas Bank water offshore [*Shelton and Hutchings*, 1990]. Associated with the shelf-edge front, a geostrophic, equatorward jet current, flows over the 300–400 m isobaths from the Cape Peninsula to Cape Columbine [*Bang and Andrews*, 1974; *Boyd and Nelson*, 1998; *Nelson*, 1985; *Shannon and Nelson*, 1996].

As part of a regional BENEFIT (Benguela Environment and Fisheries Interactions and Training) program, monthly ship-based monitoring of oceanographic and biological conditions along the St. Helena Bay Monitoring Line (SHBML) (Figure 1) was initiated in April 2000 [*Hutchings et al*., 2009a]. The aim was to determine seasonal changes in hydrography, nutrient chemistry, plankton, and pelagic fish. Using standardized techniques, monthly sampling included measurements of currents, temperature, salinity, dissolved oxygen, macronutrients (nitrate, nitrite, silicate, phosphate), phytoplankton, and mesozooplankton. This shipboard monitoring was supplemented by satellite observations, oceanographic moorings, and fisheries survey data to provide a comprehensive observational database encompassing different time and space scales relevant to oceanographic and biological processes in the Benguela. Similar sampling has been conducted along transects off Namibia and Angola [*Bartholomae and van der Plas*, 2007]. The current study presents monthly climatologies of 11 years of hydrographic data along the SHBML and investigates the monthly cross-shelf variability of oceanographic conditions. The following key questions were addressed: (1) what are the mean monthly patterns of temperature and dissolved oxygen along the SHBML? (2) Are there significant seasonal and cross-shelf differences in these parameters?

## 2. Data and Methods

Hydrographic sampling at 12 stations along the SHBML, and at stations 21 and 22 off Cape Columbine (Figure 1), has been carried out once a month from April 2000 to December 2011. The transect was orientated perpendicular to the coast off Eland's Bay, extended approximately 187 km offshore, and was sampled to a maximum depth of 1466 m at station 12. At all stations, Conductivity-Temperature-Depth (CTD) casts were conducted from the surface to within 5–10 m of the seafloor, measuring temperature, salinity, and dissolved oxygen. Throughout the 11 year period, sampling was conducted using three different research vessels and multiple SeaBird Electronics SBE 911+ CTD systems and sensors. Collection and processing of CTD data was done according to internationally accepted standards, and temperature measurements had an accuracy of $\pm 0.001$°C, while salinity had an accuracy of $\pm 0.002$ psu. During each cruise, dissolved oxygen concentrations of discrete seawater samples from selected depths were determined by Winkler titrations, and used to calibrate dissolved oxygen profiles, yielding an accuracy of $\pm 0.05$ mL $L^{-1}$ [*Carpenter*, 1965; *Carritt and Carpenter*, 1966].

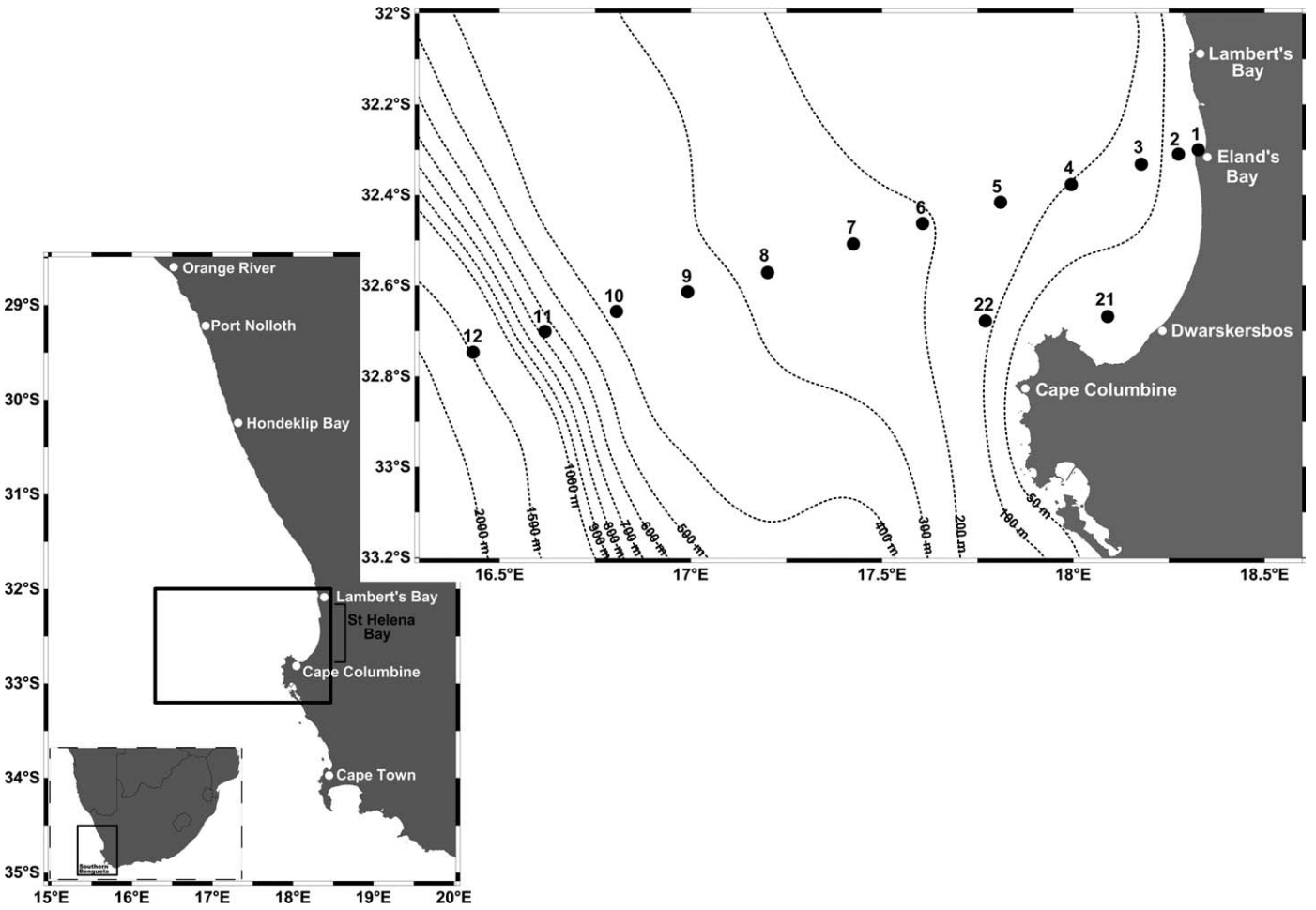


**Figure 1.** Map showing station locations in St. Helena Bay. ETOPO1 bathymetry contours are indicated as dotted lines.

Vertical profiles of temperature and salinity were used to calculate conservative temperature (°C) and absolute salinity ($S_A$ [g kg$^{-1}$]), following the new thermodynamic equation of seawater [*IOC et al*., 2010]. Time series of conservative temperature, absolute salinity, and dissolved oxygen were generated and used to compute monthly climatologies of these variables at each station. The vertical distribution of water masses was determined according to Conservative Temperature, Absolute salinity, and density layers, as illustrated in Figure 2. Modified Upwelled Water (MUW) was defined according to *Duncombe Rae* [2005], while Oceanic Surface Water (OSW), light South Atlantic Central Water (lSACW), South Atlantic Subtropical Mode Water (SASTMW), and Subantarctic Mode Water (SAMW) were defined according to *Donners et al*. [2005]. The upper limit of Antarctic Intermediate Water (AAIW) was defined as $\gamma^n = 27.12$ kg m$^{-3}$ [*Donners et al*., 2005; *Stramma and England*, 1999], while the lower limit was taken as $\gamma^n = 27.55$ kg m$^{-3}$ [*Heywood and King*, 2002; *Núñez-Riboni et al*., 2005; *You*, 2002]. Upper Circumpolar Deep Water (UCDW) was defined as $\gamma^n > 27.55$ kg m$^{-3}$, according to *Heywood and King* [2002].

Spectral analysis was performed on the monthly values of temperature, salinity, and dissolved oxygen at the surface (10 m) and bottom, according to the techniques described by *Jenkins and Watts* [1968] and *Emery and Thomson* [2001]. For each station, power spectra were computed to determine the dominant periodicities. To investigate the connectivity between temperature and oxygen across the shelf, the coherency and phase spectra between station 1 and the other stations were calculated. For this analysis, the time series at station 1 were used as the first input series in the bivariate cross-correlation function.

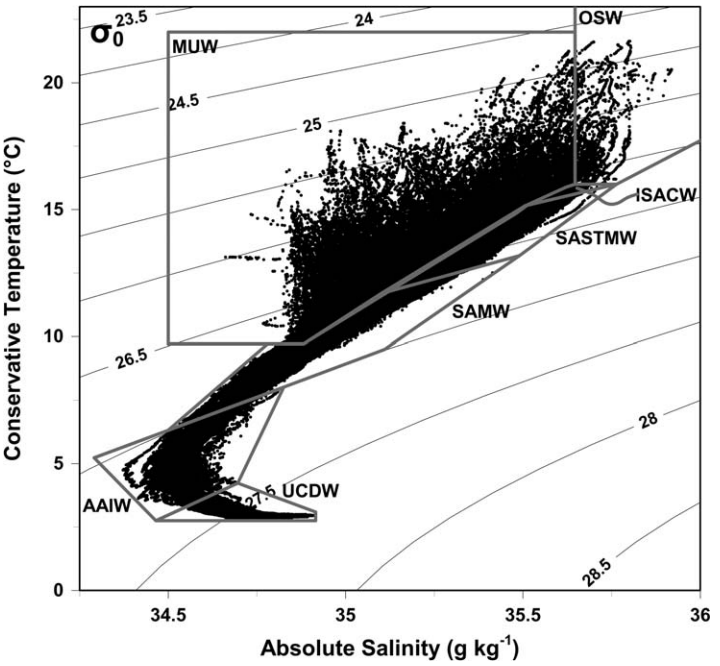


**Figure 2.** Conservative temperature (°C)—absolute salinity (g kg$^{-1}$) relationship for the SHBML transect, as well as stations 21 and 22. Water masses are indicated by gray boxes (OSW—Oceanic Surface Water, MUW—Modified Upwelled Water, LSACW—Light South Atlantic Central Water, SASTMW—South Atlantic Subtropical Mode Water, SAMW—Subantarctic Mode Water, AAIW—Antarctic Intermediate Water, and UCDW—Upper Circumpolar Deep Water).

## 3. Results

### 3.1. Temperature and Salinity

In the surface layers, most offshore stations along the SHBML transect showed elevated temperatures during spring and summer, while lower temperatures were observed in autumn and winter (Figure 3). In contrast, temperatures in the surface layers at the nearshore stations, particularly at stations 1 and 2, showed the opposite pattern, with lower values found during spring and summer, and higher values observed in autumn and winter (Figure 3). Mean monthly salinity distributions (data not shown) indicated elevated salinities in the surface layers at offshore stations during spring and summer, while salinities during autumn and winter were slightly lower. Similar to the temperature distribution, a contrasting pattern in the surface salinities was observed at nearshore stations, with higher salinities in autumn and winter, and lower values during spring and summer. At a depth of 10 m, the seasonal ranges in temperature and salinity were 4.21°C and 0.19 g kg$^{-1}$ at station 12. Temperature minima were observed during July and August, while maxima were noted in January and February (Figure 3). Salinity minima were found in April and July, with maxima occurring during January and February. At station 1, the seasonal ranges were much smaller, amounting to 2.12°C and 0.09 g kg$^{-1}$ for temperature and salinity, respectively. Minimum temperatures at station 1 were observed during February (Figure 3), while minimum salinity was noted in November, and the maximum temperature and salinity was found in June. A similar pattern of elevated temperatures and salinities during autumn and winter, and lower values in spring and summer were observed further south, off Cape Columbine, at stations 21 and 22 (Figures 4a and 4d).

Subsurface, the seasonal differences were greatly reduced, and a change in the timing of temperature and salinity minima and maxima was evident. At a depth of 300 m, the seasonal temperature ranges were 1.25°C and 0.79°C, at stations 12 and 9, respectively, while the salinity range was 0.15 g kg$^{-1}$ at station 12 and 0.07 g kg$^{-1}$ at station 9. Minimum temperature and salinity was observed at station 12 during April, while two temperature and salinity minima were observed in January and August at station 9 (Figure 3). Maximum temperature at 300 m was found in December at station 12, while maximum salinity was seen in October. At station 9, two maxima in temperature and salinity were observed during May and November. Lower down the water column, a further reduction in seasonal differences was observed. At 600 m, temperature and salinity ranges were 0.54°C and 0.06 g kg$^{-1}$, respectively, at station 12. While temperature minima and maxima were observed during April and October, respectively (Figure 3), the pattern was even less clear for salinity, with three minima in March, July, and December, and three maxima in January, April, and September.

Based on the definitions illustrated in Figure 2, seven different water masses were identified across the shelf. In the surface layers, Modified Upwelled Water (MUW) was associated with large temperature and salinity ranges between 9.71 and 21.3°C and 34.661 and 35.647 g kg$^{-1}$, while Oceanic Surface Water (OSW) was characterized by temperatures and salinities exceeding 16°C and 35.647 g kg$^{-1}$ (Figure 2). Central Waters were composed of three distinct water masses, namely Light South Atlantic Central Water (LSACW),

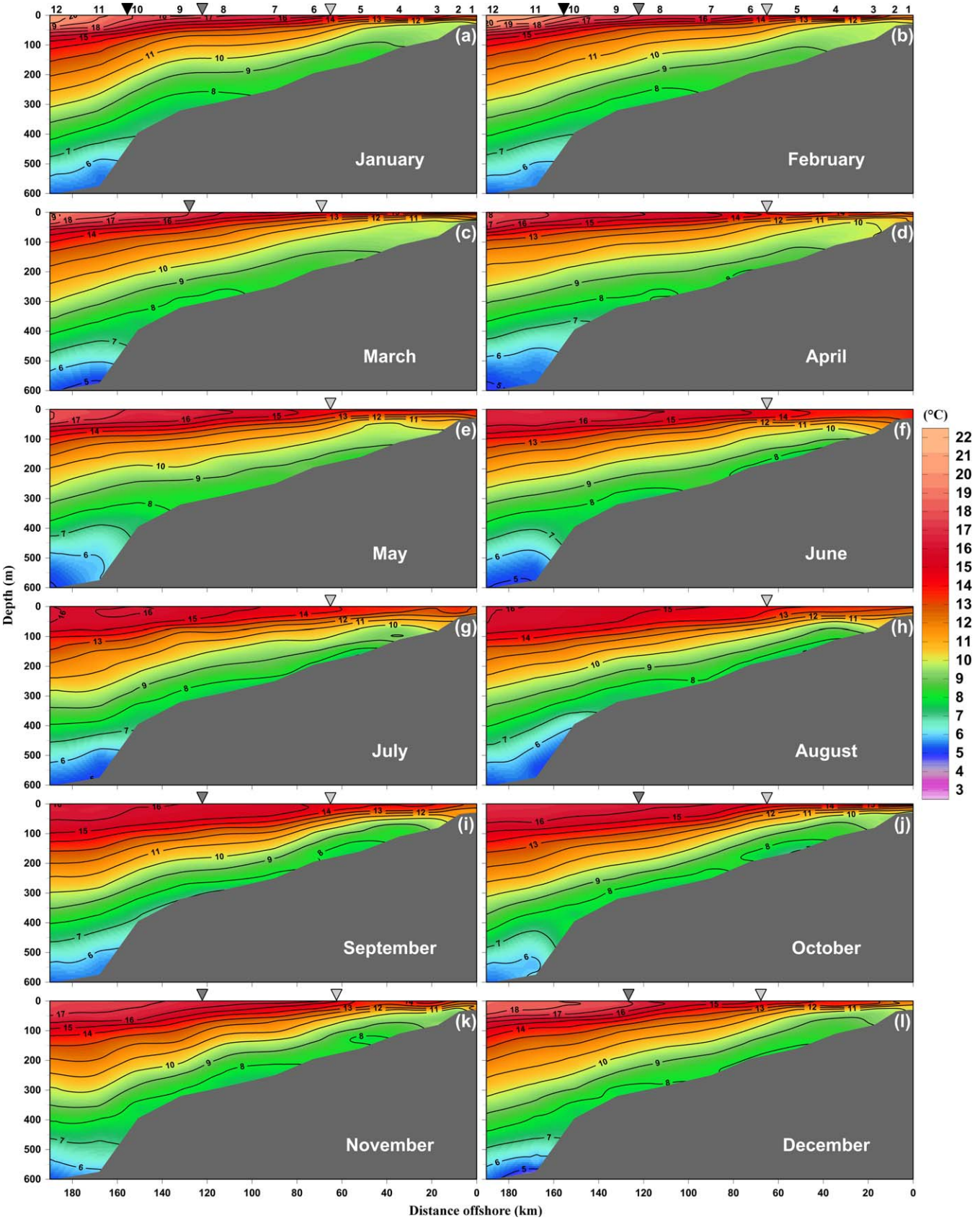


**Figure 3.** Monthly climatology of the vertical distribution of conservative temperature (°C) along the SHBML transect. Inverted triangles indicate the approximate locations of the oceanic front (black), the shelf-break front (dark gray), and the Columbine front (light gray).

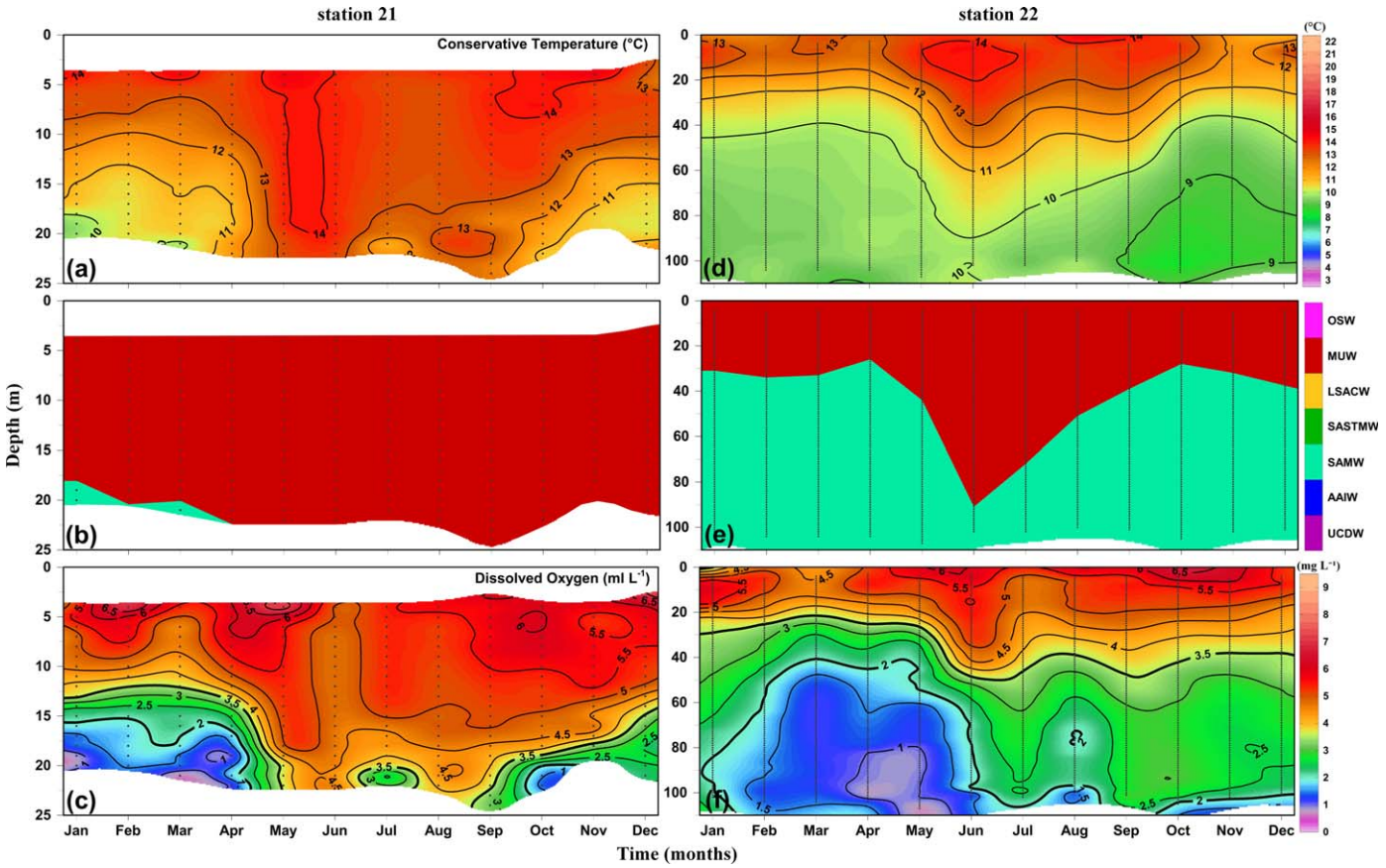


**Figure 4.** Monthly climatology of the vertical distribution of (a and d) conservative temperature (°C), (b and e) water masses, and (c and f) dissolved oxygen (mL $L^{-1}$), at stations 21 and 22 (OSW—Oceanic Surface Water, MUW—Modified Upwelled Water, LSACW—Light South Atlantic Central Water, SASTMW—South Atlantic Subtropical Mode Water, SAMW—Subantarctic Mode Water, AAIW—Antarctic Intermediate Water, and UCDW—Upper Circumpolar Deep Water).

South Atlantic Subtropical Mode Water (SASTMW), and Subantarctic Mode Water (SAMW). Temperatures of 15.15–16°C and salinities of 35.506–35.764 g $kg^{-1}$ were typical of LSACW, while SASTMW was defined by temperatures and salinities ranging between 11.69–16°C and 35.49–35.764 g $kg^{-1}$, respectively. SAMW was associated with temperatures between 6.32°C and 13.18°C and salinities of 34.78–35.49 g $kg^{-1}$ (Figure 2). Antarctic Intermediate Water (AAIW) had temperatures of 2.75–8°C and salinities between 34.29 and 34.825 g $kg^{-1}$, while Upper Circumpolar Deep Water (UCDW) had temperatures below 4.23°C, over a salinity range of 34.696–34.916 g $kg^{-1}$ (Figure 2).

The mean monthly vertical distributions of these water masses along the SHBML transect are presented in Figure 5, while the water masses at stations 21 and 22 are shown in Figures 4b and 4e, respectively. MUW occupied the top 30–100 m of the water column at most stations, extending deeper during winter (June–August) and spring (September–November), while in summer (December–February) and autumn (March–May), its vertical extent was more restricted (Figures 4e and 5a–5l). Offshore, at stations 11 and 12, OSW was found in the surface layers from November to February, with the MUW subducting beneath it most notably during January and February (Figures 5a, 5b, 5k, and 5l). LSACW was observed as a thin layer at a depth of ~80 m at stations 11 and 12 from September to January (Figures 5a and 5i–5l). SASTMW was found throughout the year at stations 6–12, occupying 1–120 m of the water column at depths between 81 and 201 m. The vertical extent of SASTMW was greater during spring and summer, and more restricted during autumn and winter, when it occupied a thinner layer of the water column (Figures 5a–5l).

SAMW was present at stations 4–12 (Figure 5), and at station 22 (Figure 4e), throughout the year. While SAMW formed the bottom layer at stations 4–9 throughout the year, seasonal variation in the vertical and shoreward extent of SAMW was evident. During spring (October) and late summer-early autumn (February

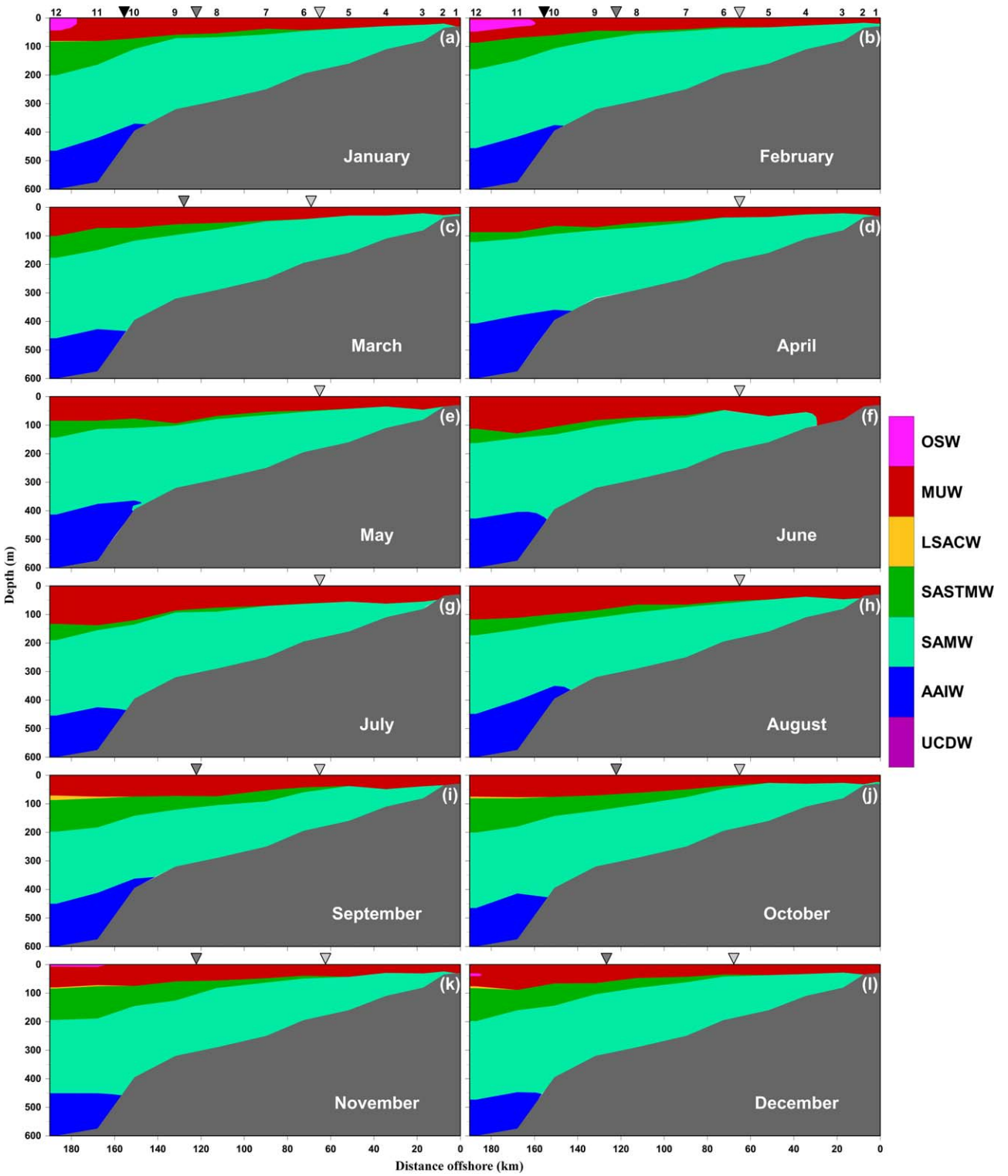


**Figure 5.** Monthly climatology of the vertical distribution of water masses along the SHBML transect (OSW—Oceanic Surface Water, MUW—Modified Upwelled Water, LSACW—Light South Atlantic Central Water, SASTMW—South Atlantic Subtropical Mode Water, SAMW—Subantarctic Mode Water, AAIW—Antarctic Intermediate Water, and UCDW—Upper Circumpolar Deep Water). Inverted triangles indicate the approximate locations of the oceanic front (black), the shelf-break front (dark gray), and the Columbine front (light gray).

and March), SAMW extended further shoreward and occupied the bottom layers at stations 1 and 2 (Figures 5b, 5c, and 5j), while at station 21 (Figure 4b), SAMW was observed in the bottom layer from mid-summer to mid-autumn (January–April). Although SAMW was observed at station 3 for most of the year, during June it penetrated only as far inshore as station 4 (Figure 5f). AAIW was observed throughout the year at stations 11 and 12, and during most months at station 10. Interestingly, AAIW was absent at station 10 during early autumn (March), early to mid-winter (June and July), and mid-spring to early summer (October–December) (Figures 5c, 5f, 5g, and 5j–5l). At station 12, the vertical extent of AAIW was least during December, when it occupied a 414 m thick layer between depths of 473 and 887 m, and greatest during June, when it occupied a 500 m thick layer between depths of 427–927 m. UCDW was observed below AAIW at station 12 only (Figure 2). In order to maintain vertical resolution at the shallow nearshore stations, the vertical distribution of water masses has been illustrated to a maximum depth of 600 m, and thus the full vertical extent of AAIW and UCDW is not visible in Figure 5. In accordance with the findings of *Duncombe Rae* [2005], AAIW was limited to the continental slope and shelf edge and did not appear to impact the shelf region significantly (Figure 5). Thus, the vertical and seasonal variations in AAIW and UCDW have not been discussed in detail.

As described earlier, substantial cross-shelf differences and seasonal variations of temperature (Figure 3) and salinity were evident. While the water mass analysis (Figure 5) revealed two distinct water masses in the surface layers across the shelf, and highlighted some variations in the spatial extent of these water masses, it did not fully capture the changes in temperature and salinity between the nearshore, midshelf, and offshore regions. For this reason, cross-shelf variations in temperature and salinity were further investigated through the use of mean monthly Temperature/Salinity (T/S) diagrams (Figure 6). Although the same water masses, as illustrated in Figure 2, were identified, Figure 6 clearly demonstrates considerable seasonal variability in MUW across the shelf.

From mid-autumn (April) to late winter (August), two distinct clusters of stations were observed (Figures 6d–6h), separated by the shelf-break front, which was identified by the surface expression of the 15°C isotherm (Figures 3d–3h). Nearshore stations, shallower than 200 m (1–5, 21, and 22), formed the first cluster, while the second cluster was composed of stations 6–12 (Figures 6d–6h). At the onset of the upwelling season in September, there was some evidence that near-surface waters at station 6 became more distinguished from other offshore stations (7–12) (Figure 6i). During October, the separation of station 6 from the nearshore (1–5, 21, and 22) and offshore (7–12) stations was more well defined (Figure 6j). Throughout the rest of the spring and summer upwelling season, there was further distinction in the MUW, with three well-defined groups of stations evident. The first cluster included nearshore stations (1–5, 21, and 22), while the second included stations 6, 7, and 8, and the third group was composed of stations 9–12 (Figures 6a, 6b, and 6j–6l). Separation between the nearshore and midshelf (6–8) stations was indicated by the Columbine front along the 200 m isobath (15°C isotherm), while the shelf-break front (17°C isotherm) distinguished midshelf stations from those further offshore (9–12) (Figures 3 and 6). During late summer (January and February), the oceanic front, represented by the 18°C isotherm, clearly separated MUW on the shelf from the OSW observed at stations 11 and 12 (Figures 5 and 6).

### 3.2. Dissolved Oxygen

Across the shelf, a large range in dissolved oxygen concentrations was observed, varying from values less than 0.5 mL $L^{-1}$ to values exceeding 6.5 mL $L^{-1}$ (Figures 4c, 4f, and 7a–7l). In the surface layers, at all stations, oxygen exceeded 4.5 mL $L^{-1}$ throughout the year, with higher concentrations observed during the spring and summer upwelling season, as well as during late autumn-early winter (Figure 4c, 4f, 7a, 7b, and 7i–7l). Low oxygen values (<3.5 mL $L^{-1}$) were observed throughout the year, confined to the bottom layers at nearshore and midshelf stations. During early to mid-spring (September and October), oxygen-depleted water (<3.5 mL $L^{-1}$) was detected only as far offshore as station 5 (Figures 7i and 7j). From early summer (December), this oxygen-depleted water extended further offshore, and was observed as far offshore as station 8 during autumn and winter (March–August) (Figures 7c–7h).

At station 3, oxygen concentrations less than 2 mL $L^{-1}$ were detected below a depth of 50 m throughout the year. During spring and summer, these low values were seen to extend higher up the water column, reaching and being maintained at a depth of 30 m from mid-summer to mid-autumn (January–April). This hypoxic (<2 mL $L^{-1}$) water extended shoreward and offshore throughout the upwelling season, reaching

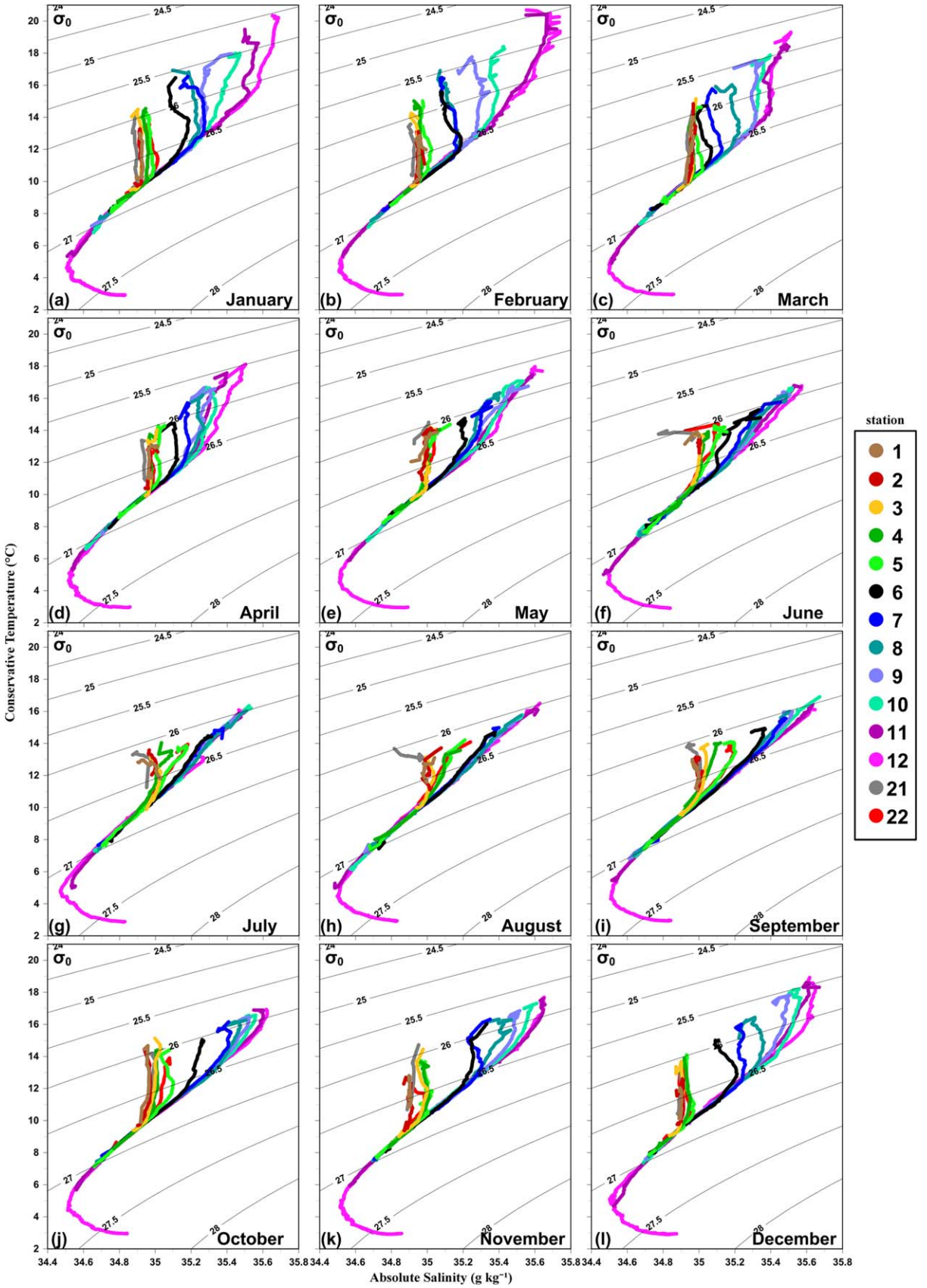


**Figure 6.** Monthly climatology of the conservative temperature (°C)—absolute salinity (g $kg^{-1}$) relationship for the SHBML transect, as well as stations 21 and 22.

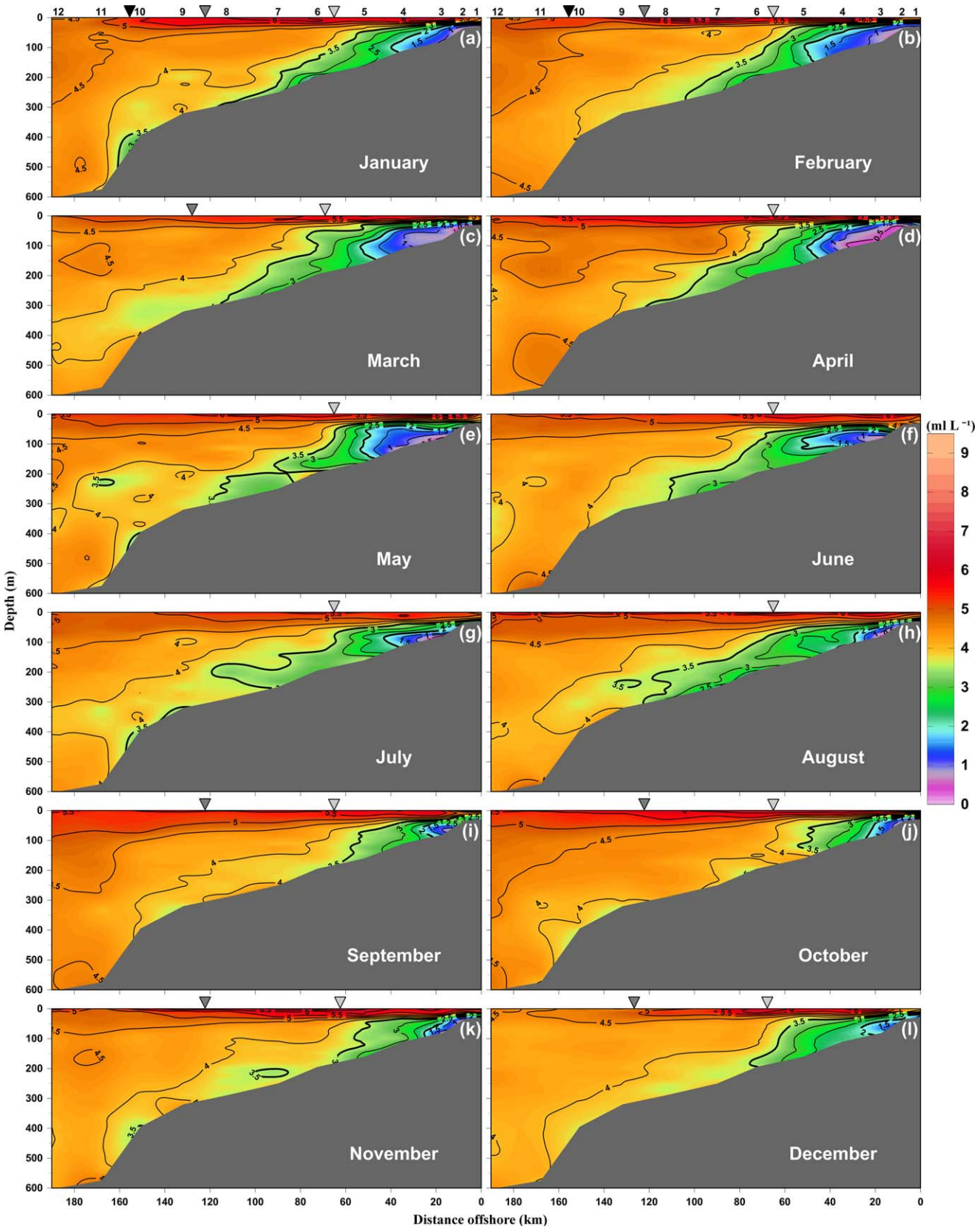


**Figure 7.** Monthly climatology of the vertical distribution of dissolved oxygen (mL $L^{-1}$) along the SHBML transect. Inverted triangles indicate the approximate locations of the oceanic front (black), the shelf-break front (dark gray), and the Columbine front (light gray).

maximal extent during late summer and autumn (Figures 7a–7e). At nearshore stations 1 and 2, hypoxic water was observed from the onset of upwelling in September through to the end of the upwelling season in April (Figure 7), while at station 21, seasonal hypoxia commenced a month later, during October (Figure 4c). Further offshore, at station 4, hypoxic water was present during most months of the year, except from October to December, while at station 5, oxygen $<2$ mL $L^{-1}$ was observed during March and May only (Figure 7).

The relationship between temperature and oxygen revealed two distinctly different linear patterns (Figure 8). The first relationship showed very little change in oxygen over a wide range of temperatures throughout the water column in the offshore region, particularly at stations 9–12 (Figures 8a–8l). Some seasonal variation in oxygen was evident in the surface and bottom layers at these stations. In the surface layers, at temperatures above 14°C, oxygen concentrations tended to be slightly higher during autumn and winter, while in the bottom layers, at temperatures below 4°C, the oxygen content of UCDW indicated slightly lower concentrations during autumn and winter, with elevated values observed during spring and summer (Figures 8a–8l).

The second pattern showed a clear linear relationship, with oxygen concentrations increasing linearly with an increase in temperature. This strong positive relationship was observed at nearshore stations (1, 2, 3, and 21) throughout the year, with persistent hypoxia prevalent in the bottom waters at station 3. Seasonal change was observed in the bottom waters at stations 1, 2, and 21, from oxygen depletion during mid-winter to early spring (July–September) to hypoxia, occurring from mid-spring to mid-autumn (October–April). During May and June, the bottom waters at these stations were well oxygenated (Figures 8a–8l). Similarly, the bottom waters at stations 4, 5, and 22 were oxygen depleted from August to December, while hypoxia was observed from mid-summer to mid-winter (January–July). Further offshore, less seasonal variability was observed in the oxygen content of the bottom waters at stations 6, 7, and 8. While these bottom waters were well oxygenated during spring, they showed oxygen depletion from summer to winter (December–August) (Figures 8a–8l).

In the surface layers, where temperature and oxygen values were highest, substantial seasonal differences were evident between the offshore stations and those closer to the coast. During winter, the cross-shelf differences between the inshore and offshore environment were less obvious (Figures 8f–8h). The contrasts were far more distinct from spring to autumn, with the greatest differentiation observed in late summer (February), when oxygen concentrations at offshore stations were $\sim$5 mL $L^{-1}$ and those at nearshore stations exceeded 7 mL $L^{-1}$ (Figure 8).

### 3.3. Spectral Analysis

Since the ship-board CTD profiles rarely provided good measurements at depths shallower than 5 m (see Figure 4c), temperature, salinity, and oxygen values from a depth of 10 m were selected to represent the surface. At each station, the bottom varied according to the bathymetry, and values from within 10–15 m of the seafloor were selected to represent the bottom layers at stations 1–6, 21, and 22. Further offshore, at stations 7–10, the bottom layers were represented by measurements from within 20 m of the seafloor, while at stations 11 and 12, measurements from depths of 540 and 650 m, respectively, were used. Surface and bottom salinity showed very low spectral energy ($<0.25$ [g $kg^{-1}$]$^2$ cycles $month^{-1}$) across the entire frequency spectrum, and although the energy peaks were at similar frequencies to those observed for temperature, they were below the 95% confidence interval and greater than the bandwidth, so were not considered significant. For this reason, salinity results have not been presented. Autospectra of the monthly temperature measurements at the surface and bottom of each station are shown in Figures 9 and 10, respectively, while autospectra of surface and bottom monthly oxygen are illustrated in Figures 11 and 12, respectively.

The dominant energy in surface temperature is evident at a frequency of 0.083 cycles $month^{-1}$ (12 month period) at all stations except stations 4 and 5 (Figures 9a–9d). Interestingly, notable cross-shelf differences in spectral energy at the 12 month period were observed, with high energy at nearshore stations (1–3, 21, and 22) (Figures 9a and 9d), lower energy in the midshelf region (stations 4–8) (Figure 9b), and substantially higher energy further offshore, particularly at stations 11 and 12 (Figure 9c). Further investigation of the coherency and phase differences (data not shown) between station 1 and the others revealed notable differences between the offshore stations and those closer to the coast. At a period of 12 months, reasonably

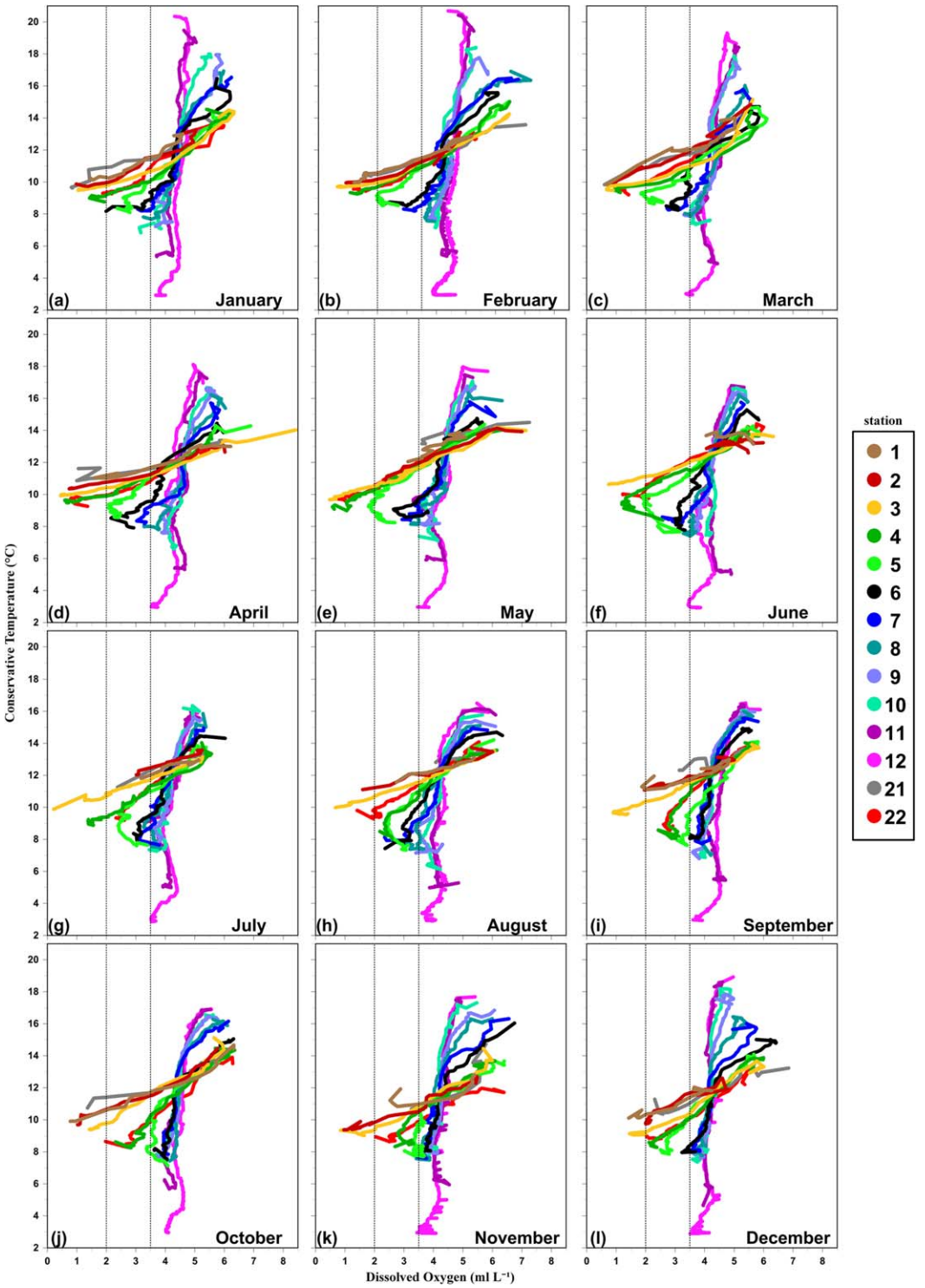


**Figure 8.** Monthly climatology of the conservative temperature (°C)—dissolved oxygen (mL $L^{-1}$) relationship for the SHBML transect, as well as stations 21 and 22. Vertical dotted lines indicate oxygen concentrations of 2 and 3.5 mL $L^{-1}$, respectively.

high coherency ($K^2 > 0.50$) was observed between station 1 and other nearshore stations (2, 3, 6, 21, and 22), with an average negative phase difference of 1.5 months. However, with a Nyquist frequency of 0.5 cycles per month, this lag is not considered significant, and implies that the annual temperature signal permeated throughout the nearshore waters. For the offshore stations, the coherency between station 1 and

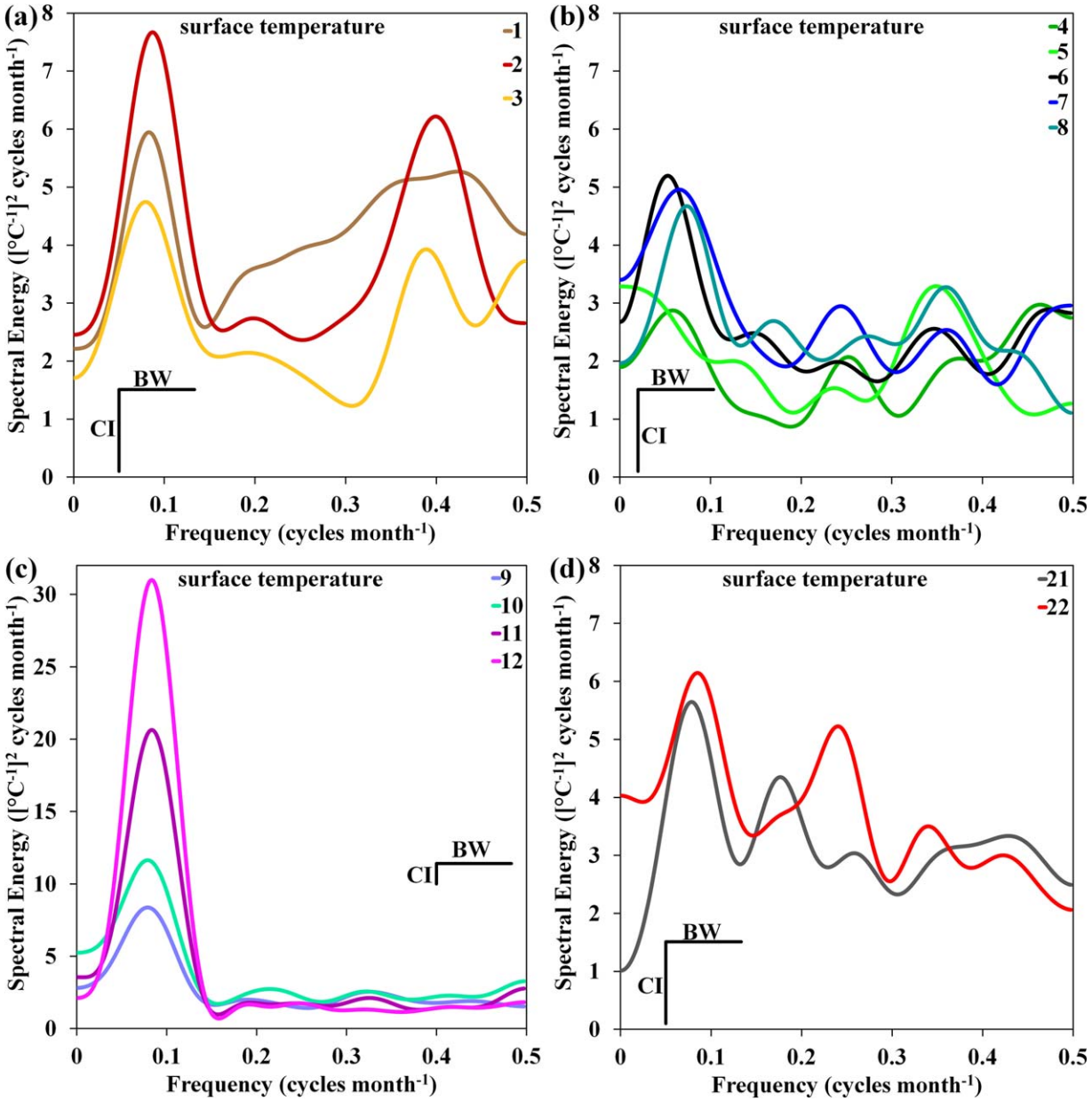


**Figure 9.** Spectral energy of the surface temperature at all stations along the SHBML transect, as well as stations 21 and 22 (BW—bandwidth and CI—confidence interval). Note the different *y* axis range for Figure 9c.

stations (7–12) was relatively weak ($K^2 < 0.3$) and the phase differences were positive with a time lag of 3.1 months. This indicated that the annual signal was observed first at the offshore stations and then propagated toward the nearshore region.

Another interesting feature in the surface temperature spectra was the significant energy peak observed at stations 2, 3, 4, and 5, at frequencies between 0.35 and 0.4 cycles month$^{-1}$ (2.5–3 month period) (Figures 9a and 9b), and at a frequency of 0.24 cycles month$^{-1}$ (4 month period) at station 22 (Figure 9d). Although the signal at the 2.5–3 month period was not statistically significant at station 1, it was clear that station 1 also exhibited elevated energy at this period (Figure 9a). There was a reasonably strong coherency ($K^2 > 0.5$) between this intraannual signal at stations 2, 3, and 22, while slightly weaker coherency ($K^2 < 0.25$) was observed between stations 2 and 5. Negative phase differences indicated that this signal was observed at station 2 before the others, although an average of 1 month is not considered significant. Similar peaks

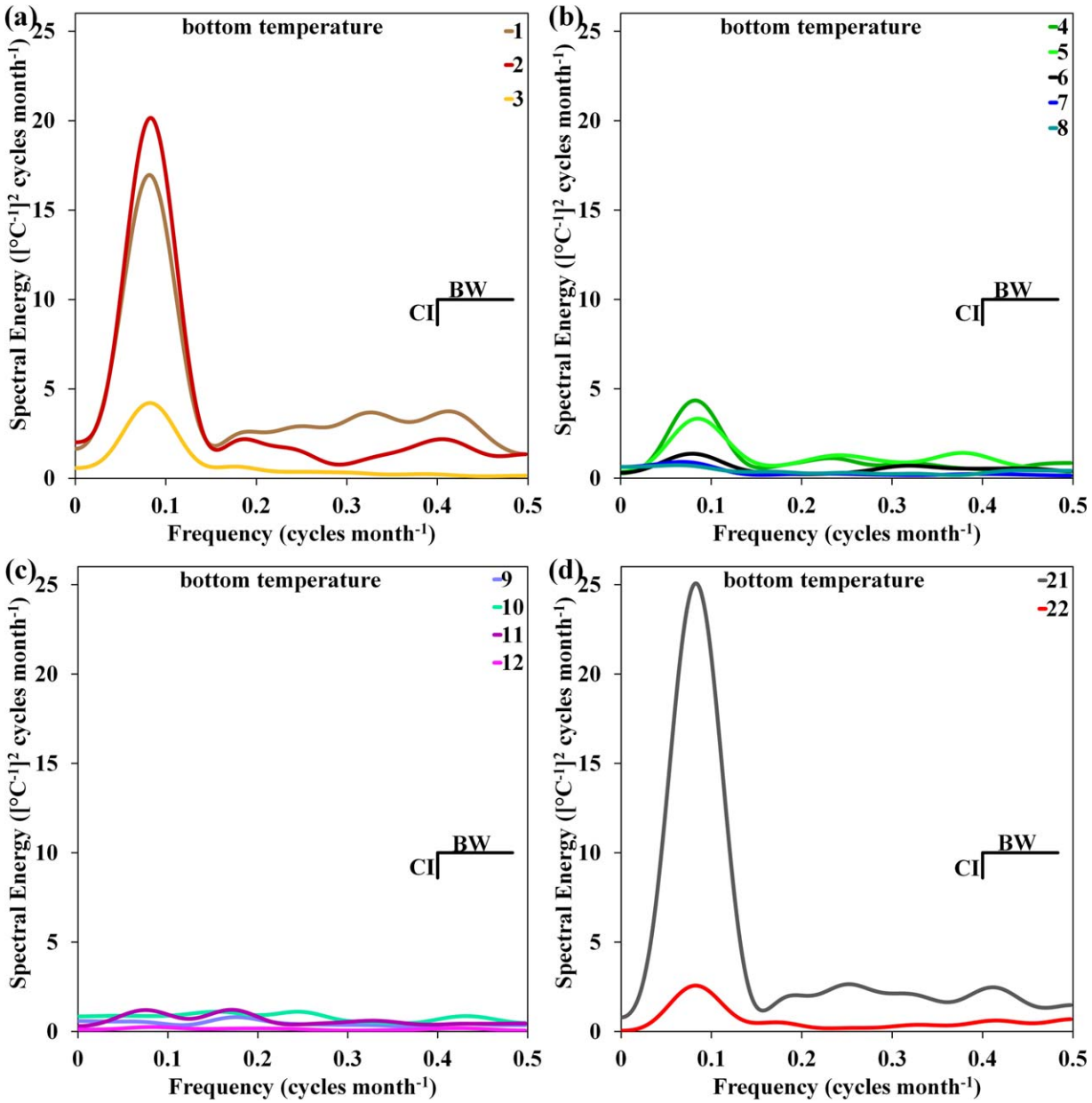


**Figure 10.** Spectral energy of the bottom temperature at all stations along the SHBML transect, as well as stations 21 and 22 (BW—bandwidth and CI—confidence interval).

were not observed at the offshore stations (6–12) (Figures 9b and 9c) and thus it is likely that this represents a coastal phenomenon.

Bottom temperature also showed significant energy peaks at a frequency of 0.083 cycles month$^{-1}$ at nearshore stations 1–5, 21, and 22, while no substantial peaks at this frequency were observed further offshore at stations 6–12 (Figures 10a–10d). Very high coherency ($K^2 > 0.68$) was observed between station 1 and stations 2–5, 21, and 22. The phase differences between station 1 and the others varied from positive to negative with lags of between 1 and 2 months, which were not considered to be significant. This result was similar to the surface temperature and implied that surface and bottom temperatures in the nearshore region varied in concert at the annual period.

Although the signatures in spectral energy of the surface and bottom oxygen showed some similarity to those observed in temperature, some obvious differences were evident. At the surface, oxygen showed

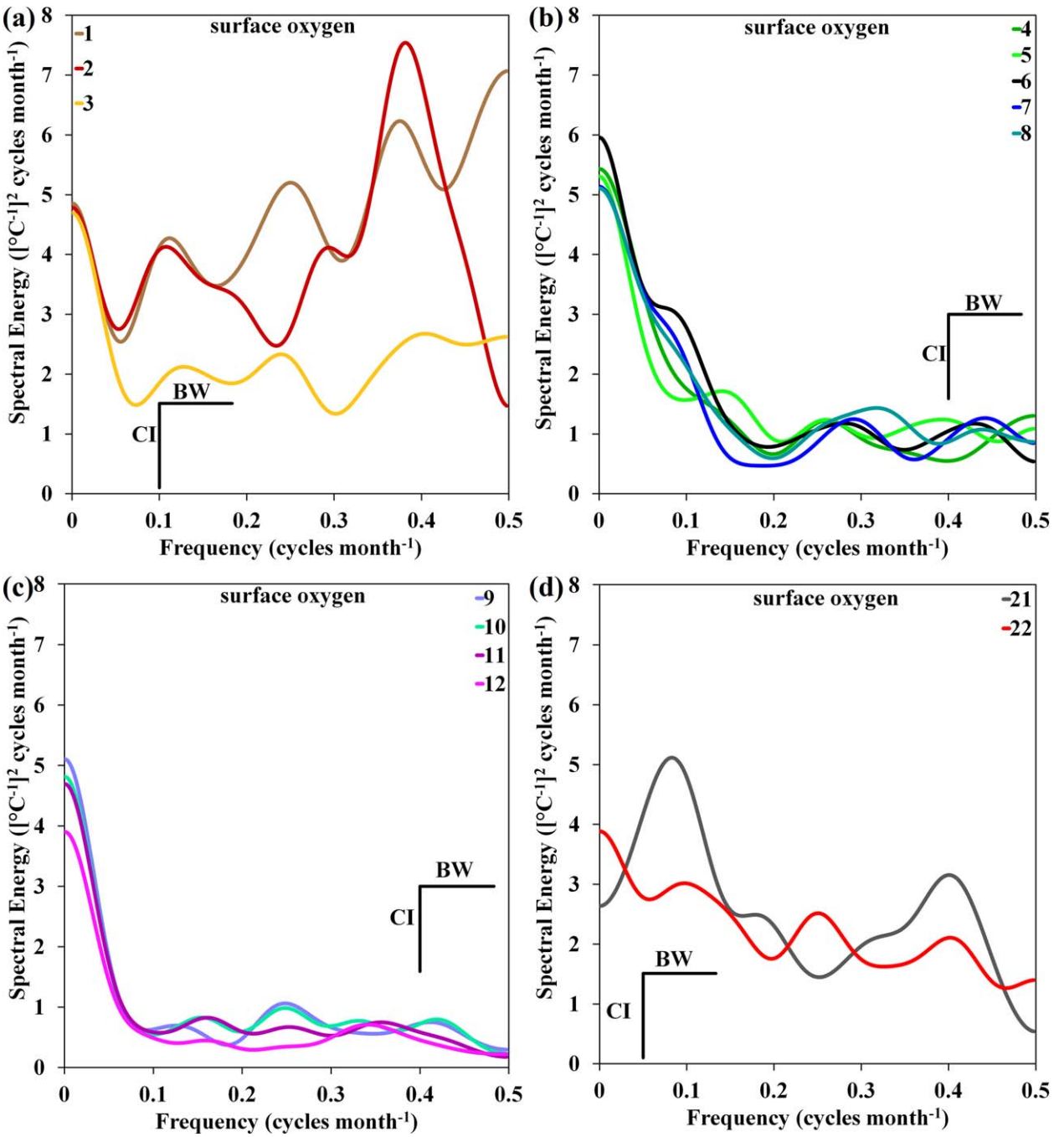


**Figure 11.** Spectral energy of the surface oxygen at all stations along the SHBML transect, as well as stations 21 and 22 (BW—bandwidth and CI—confidence interval).

significant energy at periods of 12 and 3 months at nearshore stations 1, 2, 21, and 22 (Figures 11a and 11d). In contrast to the temperature patterns, surface oxygen at all stations, except station 21, showed substantial energy at low frequencies (periods much longer than 12 months) (Figures 11b and 11c). While the coherency between stations 1 and 2 was relatively high ($K^2 > 0.59$) at both the 12 and 3 month periods, the coherency between station 1 and those further south (stations 21 and 22) was much lower ($K^2 < 0.3$). Phase differences between station 1 and the others were negative at both the 12 and 3 month periods, but the time lag of about 1 month was not significant.

Bottom oxygen showed prominent energy peaks at a period of 12 months at stations 1, 2, 4, 5, 21, and 22 (Figures 12a, 12b, and 12d), while no substantial peaks were noted at station 3, and further offshore at

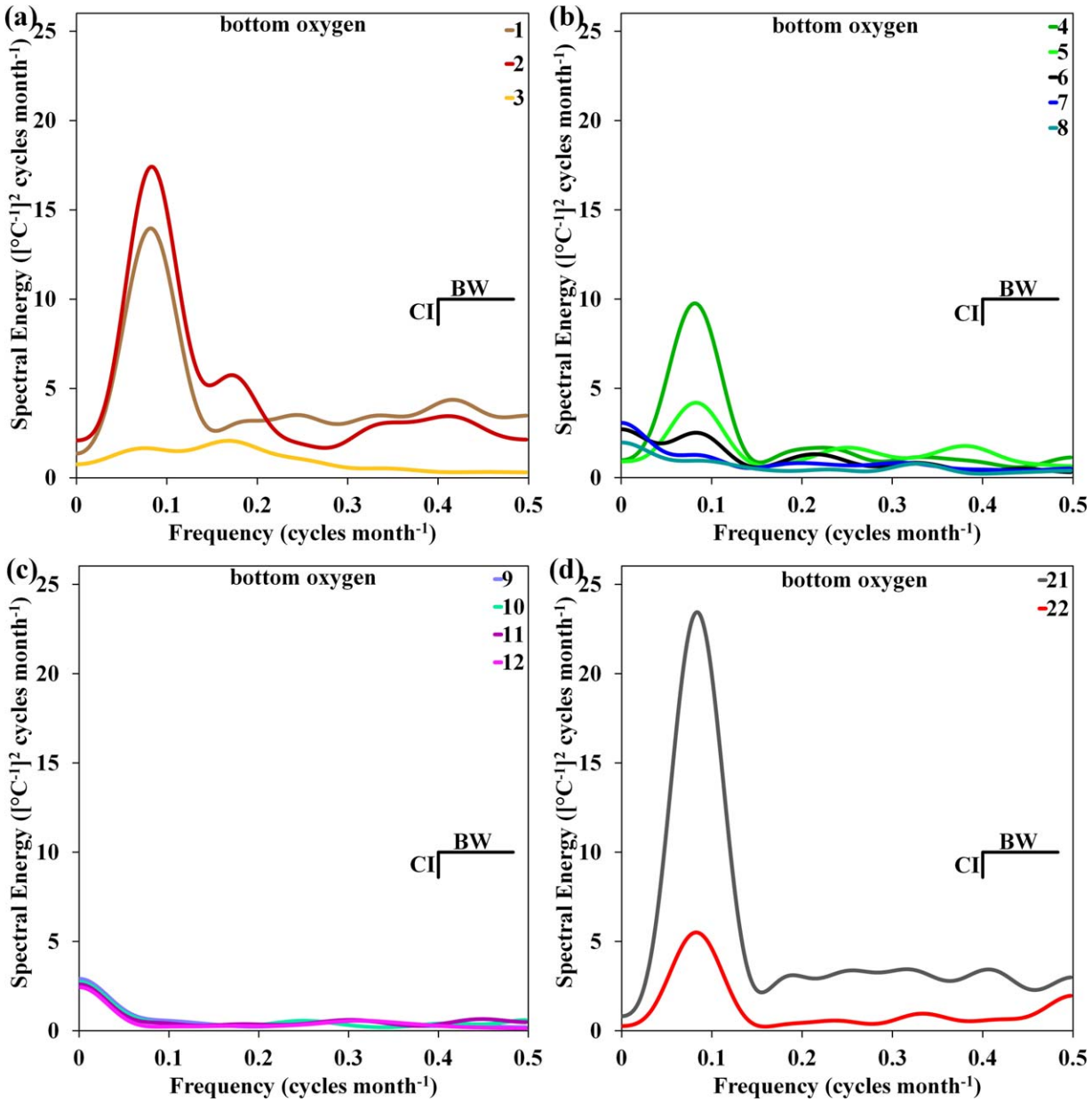


**Figure 12.** Spectral energy of the bottom oxygen at all stations along the SHBML transect, as well as stations 21 and 22 (BW—bandwidth and CI—confidence interval).

stations 7–12, energy was significant at low frequencies (Figures 12b and 12c). At the bottom, the coherency in the annual signal ($K^2 > 0.61$) between stations 1, 2, 4, 5, 21, and 22, was higher than that observed for oxygen at the surface. There was no significant time lag between these stations.

## 4. Discussion

### 4.1. Circulation and Water Masses

Several water masses were identified in the region, including Subtropical surface and intermediate waters, which were found on the continental shelf and slope (Figure 5). At the top of the water column, warm, saline Oceanic Surface Water (OSW) was observed further offshore and was distinguished from Modified Upwelled Water (MUW) found across the shelf (Figure 5). Substantial seasonal variations were observed in the surface layers, with nearshore stations showing a contrasting pattern to that observed at offshore stations (Figure 3). The classic seasonal cycle of solar insolation was illustrated in the surface layers at the

offshore stations where elevated temperatures and salinities were observed in spring and summer, and lower temperatures and salinities were found during autumn and winter (Figure 3). Similar observations of the correspondence between surface temperature patterns and the seasonal cycle of solar insolation have been described by *Demarcq et al*. [2007], *Weeks et al*. [2006], and *Hardman-Mountford et al*. [2003].

In contrast to the seasonal pattern offshore, nearshore stations showed lower temperatures and salinities during spring and summer, and higher values during autumn and winter (Figures 3, 4a, and 4d), reflecting the seasonal nature of upwelling in the southern Benguela. Lower temperatures and salinities during spring and summer (Figures 3, 4a, and 4d) were coincident with more intense upwelling resulting from stronger and more frequent south-easterly winds [*Nelson and Hutchings*, 1983; *Shannon and Nelson*, 1996]. Similarly, *Pitcher and Nelson* [2006] observed that surface temperatures were highly correlated to changes in wind, with southerly winds associated with lower temperatures and periods of wind relaxation or reversal were linked to rapid increases in temperature [*Taunton-Clark*, 1985]. These findings are also in agreement with the seasonal climatologies of hydrographic properties described by *Kearns and Carr* [2003].

Differences in the spectral energy in surface temperatures (Figure 9) corroborated the contrasting patterns between the nearshore stations and those further offshore (Figure 3). While an annual signal was dominant at most stations, notable cross-shelf differences in the energy of this signal were evident (Figure 9). At nearshore stations, phase differences were insignificant, and thus the propagation of the signal could not be determined with confidence. In contrast, positive lags between the offshore and nearshore stations suggested shoreward propagation of the annual temperature signal from the open ocean. This suggested that two different processes, with the same periodicity, influenced surface temperatures along the SHBML. As illustrated in Figure 3, and described earlier, surface temperatures at offshore stations were influenced by the cycle of solar insolation, while temperatures at nearshore stations were dominated by upwelling dynamics and coastal processes.

Using a conceptual model of cross-shelf circulation during active and quiescent upwelling phases, *Barange and Pillar* [1992] proposed the formation of multiple fronts across the upwelling zone. In accordance with their findings, MUW in the surface layers along the SHBML (Figure 5) could be separated into distinct zones, divided by the shelf-break, Columbine, and oceanic fronts (Figures 3 and 6). The oceanic front is a well-defined longshore thermal front which marks the boundary between the upwelling zone and the open ocean gyre circulation [*Barange and Pillar*, 1992; *Shannon and Nelson*, 1996]. During mid to late summer, this front distinguished MUW on the shelf from the OSW found at stations 11 and 12 (Figures 6a and 6b), and MUW was observed to subduct beneath the OSW (Figures 5a and 5b). Similar observations of the sinking of upwelled water at the oceanic front have been made off the peninsula south of Cape Town [*Andrews and Hutchings*, 1980], and this mechanism has been suggested to reduce offshore advective losses of planktonic organisms [*Barange and Pillar*, 1992]. As a consequence of the wide shelf in this region, it has been observed that upwelling takes place both in a narrow strip along the coast and at the shelf break, resulting in the formation of the upwelling and shelf-break fronts [*Nelson and Hutchings*, 1983; *Shannon and Nelson*, 1996]. While the upwelling front is known to separate newly upwelled water along the coast from older upwelled water on the shelf [*Barange and Pillar*, 1992; *Nelson and Hutchings*, 1983], it could not be clearly defined in this study (Figures 3 and 6), likely due to the combined effects of the sampling resolution and the generation of monthly climatologies, which serves to mask the temperature differences between newly upwelled (9–10°C) and older upwelled water on the shelf.

South of 30°S, the Benguela Current is characterized by two flow paths [*Veitch et al*., 2010]. While the offshore flow path is located along the western edge of the Agulhas eddy corridor [*Garzoli and Gordon*, 1996], the inshore path is topographically steered by the shelf edge [*Veitch et al*., 2010]. As this inshore limb of the Benguela Current passes the Cape Columbine headland, it splits into two branches, one veering slightly north-west along the shelf edge, while the shoreward branch continues north past the Cape Columbine headland [*Shannon*, 1985; *Shannon and Nelson*, 1996; *Veitch et al*., 2010]. This bifurcation of flow north of 33°S contributes to the occurrence of shelf-break upwelling and hence the formation of the shelf-break and Columbine fronts [*Shannon*, 1985].

The Columbine front, previously identified by *Shannon* [1985], was well defined and evident throughout the year, along the 200 m isobath between stations 5 and 6 (Figure 6), marked by the 14°C isotherm in winter and the 15°C isotherm during summer (Figure 3). From September to March, the shelf-break front was

observed along the 300 m isobaths between stations 8 and 9, separating midshelf stations from those further offshore (Figures 3 and 6). During late summer, the shelf-break front could be clearly distinguished from the oceanic front, but throughout the rest of the year, there was no clear distinction between these fronts (Figures 3 and 6). Similarly, during autumn and winter, the shelf-break front could not be clearly differentiated from the Columbine front (Figures 3 and 6). A schematic diagram depicting the seasonal differences in the locations of these fronts is illustrated in Figure 13. These results agree well with the findings of *Nelson and Hutchings* [1983] and *Shannon and Nelson* [1996] who suggested that, north of Cape Columbine, these fronts merge as a result of the combined effects of surface cooling during autumn and winter, and the less intense offshore advection of surface waters. These findings also correspond to those of *Shannon et al*. [1984], who observed that from autumn to spring, surface temperature distributions tended to be more uniform and fronts were less pronounced. During spring and summer, enhanced upwelling and increased offshore advection of surface waters are likely to result in the merging of the upwelling and Columbine fronts [*Nelson and Hutchings*, 1983; *Shannon and Nelson*, 1996; *Shannon*, 1985].

The differentiation of MUW described in the current study is supported by observations of three distinct clusters of zooplankton communities across the SHBML, related to the inner bay, midshelf, and offshore zones [*Hutchings et al*., 2012]. The characterization of phytoplankton size spectra across the SHBML [*Crichton et al*., 2013] highlighted similar distinctions between the inner bay, frontal area, and offshore zones. The location of the shelf-break front, identified by the surface expression of the 17°C isotherm during summer, was, on average, 130 km offshore (Figure 3), in agreement with *Veitch et al*. [2010] who demonstrated topographic control of the shelf-break front in the southern Benguela by illustrating an exact match between the location of the annual average 17°C isotherm and the shelf edge, represented by the 300 m bathymetry contour. The seasonal variation in the temperature observed at the shelf-break front, from 15°C in autumn, winter, and spring to 17°C during summer (Figure 3), corresponds with the seasonal differences in temperature at the shelf-break described by *Veitch et al*. [2009]. Similarly, further south off the Cape Peninsula, *Shelton and Hutchings* [1990], observed an intensification of the shelf-break front during summer due to increased upwelling inshore and warmer water offshore.

Despite the merging of fronts during autumn and winter, nearshore stations (1–5, 21, and 22) remained discriminated from stations further offshore (Figures 3 and 6), illustrating that circulation dynamics within St. Helena Bay (Figure 1) consistently differed from those on rest of the shelf throughout the year. Cyclonic wind stress curl, resulting from the topographic influence of the Cape Columbine headland on the wind [*Kamstra*, 1985; *Jury*, 1985] induces the formation of a plume of upwelled water, which extends north from Cape Columbine [*Taunton-Clark*, 1985]. This plume has been observed on the landward side of the permanent baroclinic jet [*Shannon*, 1985], which is located over the 200–300 m isobaths [*Bang and Andrews*, 1974; *Buys*, 1957, 1959; *Nelson and Polito*, 1987] and contributes to the formation of the shelf-break and Columbine fronts, as observed in Figures 3, 6, and 13 and in *Shannon* [1985]. Pronounced cyclonic curvature of equatorward winds in the lee of Cape Columbine [*Jury*, 1985] is thought to influence the orientation of the jet and the upwelling plume [*Taunton-Clark*, 1985]. The absence of a significant annual signal in the surface temperature at stations 4 and 5 (Figure 9) is likely due to high short-term variability associated with the position and orientation of the jet and upwelling plume. Further north, off Lambert's Bay, the baroclinic jet was also observed to limit cross-shelf exchange, as illustrated by a clear separation between dinoflagellate blooms inshore and diatom dominated populations further offshore [*Pitcher and Nelson*, 2006]. *Penven et al*. [2000] concluded that the combined effects the wind stress curl and the topography of Cape Columbine and St. Helena Bay, resulted in the formation and maintenance of a cyclonic recirculation within the bay, which, together with the upwelling plume off Cape Columbine, tends to isolate the bay environment from the shelf region by enhancing retention and limiting the cross-shelf exchange of water. A significant intra-annual peak in surface temperature spectra at stations 2–5, and 22 (Figure 9), suggested that the cyclonic circulation within the bay is associated with a variability of 3–4 months.

In contrast to the surface layers, where the seasonal ranges of temperature and salinity were substantial (Figures 3, 4a, and 4d), seasonal variations in subsurface temperature and salinity were greatly reduced (Figures 3, 4a, and 4d). A significant annual signal in bottom temperature was limited to stations within St. Helena Bay, with no substantial peaks further offshore (Figure 9), suggesting that this signal was likely associated with the domination of upwelling dynamics and the occurrence of the cyclonic recirculation in the nearshore environment. Using hydrographic data collected along 24°S, *McCarthy et al*. [2011] made

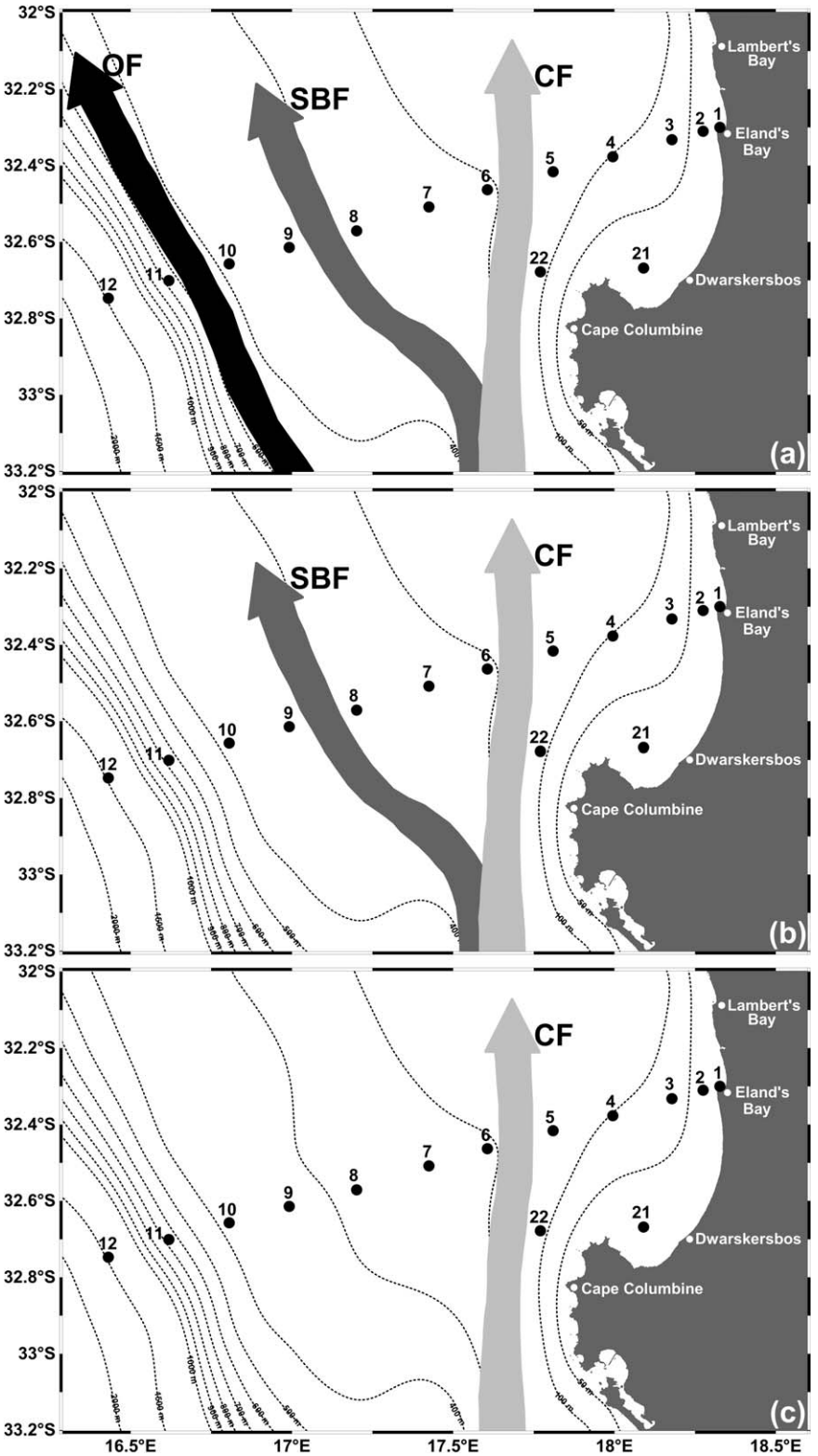


**Figure 13.** Schematic illustration of the oceanic front (OF—black), shelf-break front (SBF—dark gray), and the Columbine front (CF—light gray) during (a) January and February, (b) March and September to December, and (c) April to August.

similar observations of significant seasonal variation in the surface waters, with temperatures and salinities during October–November being up to 6°C and 0.3 psu cooler and fresher than those in February–April. While *McCarthy et al*. [2011] found that no seasonality was evident below 300 m, distinct temperature minima and maxima with a seasonal range of 0.54°C were still evident at a depth of 600 m at station 12 along the SHBML (Figure 3).

In accordance with previous descriptions of the large-scale water mass characteristics in the region [*Duncombe Rae*, 2005; *Shillington et al*., 2006; *Shannon and Nelson*, 1996], South Atlantic Central Water (SACW) on the shelf constituted the source of water which is upwelled along the coast under the influence of persistent equatorward winds (Figures 3 and 5). Based on the definitions of *Donners et al*. [2005] and *McCartney* [1982], SACW is a combination of light South Atlantic Central Water (LSACW), South Atlantic Subtropical Mode Water (SASTMW), and Subantarctic Mode Water (SAMW) (Figures 2 and 5). Using potential temperature and salinity ranges, *Provost et al*. [1999] also identified three types of subtropical mode water, and a more detailed cluster analysis by *Sato and Polito* [2014] similarly revealed three groupings of mode waters in the South Atlantic. The majority of earlier investigations, such as *Hanawa and Talley* [2001], *Provost et al*. [1999], and *Shannon and Nelson* [1996] which describe water mass characteristics in the South Atlantic Ocean have focused specifically on the geographic distribution of these water masses as well as their formation regions. While there is some information about the seasonal variation in the formation of these water masses [*Sato and Polito*, 2014], seasonal changes in their distribution have not been considered in great detail. In the current study, there was substantial seasonal variation in these water masses observed across the SHBML.

LSACW was only observed offshore, at stations 11 and 12, during spring and summer (Figure 5). LSACW is formed along the Subtropical Convergence (STC) and in the Cape Basin, and while some of it subducts in the subtropical gyre of the South Atlantic Ocean, most of it is first exported to the Indian Ocean where it recirculates and reenters the South Atlantic Ocean as Agulhas leakage [*Donners et al*., 2005; *Hanawa and Talley*, 2001; *Tomczak and Godfrey*, 2003]. It is the lightest mode water in the South Atlantic, and according to *Tomczak and Godfrey* [2003], some of the LSACW is Indian Central Water (ICW) transported into the South Atlantic via the Agulhas Retroflection. *Provost et al*. [1999] found that LSACW occupied a zonal band across the Atlantic basin, centered at 33°S. *Sato and Polito* [2014] observed that when this water mass was present as a deep mixed layer, it was more concentrated in the eastern part of the South Atlantic basin, with the thickest layers noted east of the Greenwich Meridian. When it was observed as a homogenous layer separated from the surface by the seasonal thermocline or mixed layer, the distribution spread out as far west as 48°W [*Sato and Polito*, 2014]. The spatial distribution of LSACW suggested that the Benguela Current played an important role in the advection of this mode water from east to west [*Sato and Polito*, 2014; *Stramma and England*, 1999], and it also coincided with the location of the Agulhas eddy corridor [*Garzoli and Gordon*, 1996].

SASTMW was found in the midshelf and offshore regions throughout the year, with greater vertical extent during spring and summer (Figure 5). SASTMW consists of mode waters formed mainly in the Brazil-Malvinas Confluence region, in the central part of the Atlantic basin along the South Atlantic Current, and 13°C mode water transported into the South Atlantic via Agulhas Rings [*Donners et al*., 2005; *Gordon*, 1981; *Provost et al*., 1999; *Tomczak and Godfrey*, 2003]. This is the most common mode water and is centered between 30°S and 35°S across the entire South Atlantic basin [*Provost et al*., 1999]. In contrast to the findings of *Provost et al*. [1999] and *Donners et al*. [2005], *Sato and Polito* [2014] described that this water mass was mainly restricted to the recirculation gyre of the Brazil Current, west of 25°W. The observation of SASTMW in the midshelf and offshore regions of the SHBML (Figure 5) agrees with the descriptions of *Provost et al*. [1999] and *Donners et al*. [2005], but is in contrast to those of *Sato and Polito* [2014].

SAMW comprised the bulk of Central waters on the shelf, and showed seasonal variation in its vertical and shoreward extent (Figure 5). Formation of SAMW is not spatially uniform and preferential subduction occurs at specific sites, just north of the Subantarctic Front (SAF) [*Gordon*, 1981; *Sallée et al*., 2010]. Some of this SAMW subducts within the South Atlantic, stays in the Antarctic Circumpolar Current (ACC) and reemerges further downstream, while some subducts into the subtropical gyre of the Atlantic basin [*Donners et al*., 2005; *Provost et al*., 1999]. This water mass was found to occupy a large part of the Atlantic basin between 25°S and 42°S [*Provost et al*., 1999]. While the observation of SAMW along the SHBML (Figure 5) agrees with the findings of *Provost et al*. [1999], they contradict those of *Sato and Polito* [2014], who found that this water mass occurred mainly south of 35°S.

### 4.2. Low Oxygen Water (LOW)

The southern Benguela forms part of one of the most productive upwelling ecosystems in the world, and as such, the shelf regions are subject to naturally occurring hypoxia and anoxia [*Monteiro et al*., 2011], and St. Helena Bay is the main region where LOW is generated [*Monteiro and van der Plas*, 2006]. Cross-shelf differences were substantial, with the offshore region showing little variation in water column oxygen throughout the year, while significant vertical and seasonal change was observed in the midshelf and nearshore regions (Figures 7 and 8). In contrast to the temperature, both surface and bottom oxygen spectra at stations further offshore (Figures 11 and 12, respectively) showed significant energy at periods much longer than 12 months. However, the relatively short length of the time series along the SHBML (11 years) prevents detailed discussion of this signal. Previous investigations of long-term changes in oxygen in the St. Helena Bay region have demonstrated that, while no long-term trend is evident, decadal-scale variations in oxygen occur [*Jarre et al*., 2015; *Hutchings et al*., 2012; *Pitcher et al*., 2014], and the energy peaks at low frequencies (Figures 11 and 12) may be linked to these longer-term variations.

In agreement with the findings of *Monteiro and van der Plas* [2006] and *Pitcher and Probyn* [2011], oxygen-depleted ($<$3.5 mL $L^{-1}$) water was confined to the bottom layers at nearshore and midshelf stations along the SHBML (Figures 7 and 8), driven by the buildup of decaying organic matter throughout the upwelling season. Substantial seasonal change in the extent of the oxygen-depleted water was evident, with these waters limited to the nearshore region (up to station 5) during early spring, and extending further offshore (as far as station 8) during the rest of the year (Figure 7). This also agrees with *Jarre et al*. [2015], who described a well-defined seasonal cycle of oxygen in St. Helena Bay, with a clear link to the strength of the wind-driven upwelling. Significant peaks in spectral energy at periods of 12 and 3 months observed in the surface and bottom oxygen at nearshore stations (Figures 11 and 12) illustrated that large annual and intra-annual variability in oxygen was limited to the nearshore environment. These findings are consistent with *Pitcher et al*. [2014], who also described confinement of LOW to St. Helena Bay, with high variability observed in the shallow nearshore regions. Similarly, the spatial distribution of bottom oxygen on the west coast of South Africa [*Jarre et al*., 2015] illustrated the limitation of LOW to the nearshore regions.

Persistent hypoxia ($<$2 mL $L^{-1}$) in the bottom waters at stations 3 and 4 suggested the occurrence of a permanent reservoir of LOW within St. Helena Bay (Figures 7 and 8). Within the bay, a strongly stratified two layer system, with pronounced thermoclines separating sun-warmed surface water from colder upwelled water below, is generated and maintained by the cyclonic circulation [*Pitcher and Nelson*, 2006]. Evidence of this can also be seen in Figures 4b, 4e, and 7. These conditions support high primary production fuelled by the input of new nitrate from upwelled water, which induces large fluxes of organic carbon to the bottom waters [*Bailey and Chapman*, 1985], where strong stratification coupled with microbial activity depletes the oxygen [*Monteiro et al*., 2005; *Monteiro and Roychoudhury*, 2005; *Touratier et al*., 2003]. It is likely that this interplay between local physical and biogeochemical processes [*Monteiro et al*., 2006] is responsible for the maintenance of the LOW reservoir observed at stations 3 and 4. Observations of elevated organic carbon in the surface sediments [*Bailey and Chapman*, 1985] correspond approximately to the location of stations 3 and 4 (Figure 1), and the lack of significant spectral energy peaks, reflecting the low variability in the bottom oxygen at station 3 (Figure 12a), support the observation of a permanent LOW reservoir there (Figure 7). *Monteiro et al*. [2006] proposed a two phase model of the development of LOW on the southern Benguela shelf, suggesting that a LOW reservoir develops seasonally in response to stratification, retention and upwelling-fuelled carbon fluxes. While the findings of the current study are in general agreement with the model proposed by *Monteiro et al*. [2006], the results in Figures 7 and 8, as well as observations by *Pitcher et al*. [2014], suggested that the occurrence of the LOW reservoir of hypoxic water in St. Helena Bay is more permanent than previously thought, centered around stations 3 and 4.

Seasonal shoreward and offshore expansion of the LOW reservoir occurred throughout the upwelling season, with the maximum extent observed during late summer and autumn (Figure 7). At shallow nearshore stations (1, 2, and 21), the strong linear relationship between temperature and oxygen (Figure 8) suggested shoreward advection of LOW from the reservoir at stations 3 and 4. Similar to the current study, *Pitcher et al*. [2014] also observed a strong linear relationship between temperature and oxygen at shallow nearshore stations in St. Helena Bay. Further north, off Hondeklip Bay (30°S), *Monteiro et al*. [2004] also observed that LOW variability was closely correlated to temperature, suggesting that there are advective linkages between nearshore sites along the South African west coast, north of St. Helena Bay. Similarly, observations of LOW

off the Cape Peninsula [*Andrews and Hutchings*, 1980] are believed to result from southward transport of LOW from St. Helena Bay. Shoreward transport and concentration of high biomass phytoplankton blooms commonly occurs during the upwelling season [*Pitcher and Nelson*, 2006; *Pitcher and Probyn*, 2011]. The oxygen demand resulting from the sedimentation and decay of these blooms [*Monteiro et al*., 2006; *Pitcher and Probyn*, 2011] causes severe and abrupt decreases in nearshore oxygen of up to 6 mL $L^{-1}$ at periods of 2–5 days, particularly toward the end of the upwelling season [*Pitcher et al*., 2014]. Oxygen depletion at shallow, nearshore stations is thus driven by the combined effects of the seasonal shoreward advection of LOW from the reservoir at stations 3 and 4 (Figures 4c, 4f, and 7), coupled with the local decay of phytoplankton blooms throughout the spring and summer upwelling season.

While wind mixing during winter was responsible for the reoxygenation of the entire water column at nearshore stations (1, 2, and 21), particularly during June (Figures 4c and 7), it was unable to completely erode the LOW reservoir below a depth of 50 m at station 3 (Figures 7 and 8), highlighting the stability of the bottom waters within the bay. Similarly, further south at station 22 (Figure 4f), the water below a depth of about 40 m remained depleted in oxygen throughout the year, suggesting that at this station, wind mixing during winter did not penetrate much below this depth. A time series of temperature and oxygen measurements from a depth of 70 m [*Pitcher et al*., 2014], and the lack of significant spectral energy peaks at station 3 (Figure 12a), confirms observations of the stability of the bottom waters within St. Helena Bay. While small short-term increases in oxygen were observed in relation to wind mixing events during June and July, better reoxygenation was observed during spring transitions (mid-August to late September) [*Pitcher et al*., 2014].

Further offshore, at station 4, annual variability was high (Figure 12b) and bottom waters were hypoxic during most months of the year, except from October to December (Figures 7 and 8). Similarly, the bottom waters at stations 6, 7, and 8, were well oxygenated during spring. This suggested that the influx of new SAMW during the early part of the upwelling season (Figure 5) was able to improve the oxygen conditions in the midshelf region and limit the offshore extent of hypoxic bottom waters (Figures 7 and 8). This corresponds to the findings of *Monteiro and van der Plas* [2006] and *Duncombe Rae* [2005] who suggested that the exchange of central waters between the slope and shelf off Cape Columbine tends to reoxygenate the bottom waters. The offshore expansion of hypoxic and oxygen-depleted water during the latter part of the upwelling season and throughout winter may be related to increased periods of upwelling relaxation and wind-induced mixing, as also suggested by *Pitcher et al*. [2014], but could also be due to the effects of perennial poleward flow in the nearshore and midshelf region most notably below a depth of 40 m, which has been suggested to intensify slightly during late summer and autumn [*Chapman and Shannon*, 1985; *Holden*, 1987; *Nelson and Polito*, 1987; *Shannon*, 1985]. *Nelson* [1989] alluded to the possible existence of cross-shelf compensation flow north of Cape Columbine, which may also contribute to the offshore expansion of oxygen-depleted water (Figures 7 and 8).

Hypoxia is known to significantly influence the distribution and behavior of demersal [*Atkinson et al*., 2011; *Hamukuaya et al*., 1998; K. Wieland et al., Catch rates of hake in relation to environmental conditions: An exploratory analysis for the South African west coast, unpublished report, 36 pp., CEC FP7 'ECOFISH' Project, Benguela Current Commission, 2012] and bottom fauna [*Blamey et al*., 2012; *Cockcroft*, 2001; *Cockcroft et al*., 2008]. The influence of oxygen concentrations on the distribution and condition of pelagic species has not been extensively investigated in the southern Benguela. However, recent analyses of the distributions of pelagic fish (Sardine, Anchovy, and Round Herring) in relation to environmental conditions on the South African west coast have indicated that although Sardine and Round Herring show some tolerance to oxygen concentrations as low as 2.75 mL $L^{-1}$, they all show a preference for well-oxygenated water ($>$3.5 mL $L^{-1}$) (N. Mhlongo, DAFF, personal communication, 2014). St. Helena Bay is a well-known retention area with elevated phytoplankton [*Weeks et al*., 2006] and zooplankton [*Huggett et al*., 2009] biomass, which acts as a nursery ground for numerous marine living resources. The distribution of LOW in this region is thus an important factor determining the habitable area available to these resources.

## 5. Conclusions

Substantial cross-shelf differences, as well as vertical and seasonal variations in temperature, salinity, water masses, and oxygen were observed along the SHBML transect, with seasonal differences being more substantial near the surface than in subsurface layers. Contrasting patterns between the inshore and offshore

environment illustrated the influence of different forcing mechanisms, with solar insolation dominating surface temperature changes in the offshore region, and upwelling dynamics dominating closer to the coast, and cross-shelf distinctions in MUW resulting from variations in the location of the oceanic and bifurcated shelf-break fronts. As a result of the combined influence of the cyclonic recirculation, the Cape Columbine upwelling plume, and the shelf-break and Columbine fronts, dynamics within St. Helena Bay consistently differed from those on the rest of the shelf, and may be associated with an intraannual signal with a periodicity of 3–4 months.

Although the knowledge and understanding of oceanographic variability has been extensively enhanced through the use of satellite data, as well as model output, accurate in situ measurements remain the only reliable means of investigating subsurface water column properties. The current study has demonstrated that a monthly sampling resolution adequately captures the seasonal variation in water masses and oxygen, and has highlighted the existence of an intraannual signal with a periodicity of 3–4 months in the nearshore environment, as well as a longer-term oxygen signal in the offshore region. However, a more comprehensive strategy, combining higher frequency in situ sampling at the appropriate spatial scales with high-resolution hydrodynamic and biogeochemical modeling, is required to fully understand the shorter-term fluctuations in circulation and oxygen dynamics, and the sustained implementation of such a strategy is necessary for meaningful assessment of long-term change.

**Acknowledgments**

The authors wish to thank the officers and crew of the FRS *Africana*, FRS *Algoa*, and the FRS *Ellen Khuzwayo* for their tireless support during the cruises, as well as all the scientific and technical staff at the South African Department of Environmental Affairs (DEA), Branch: Oceans and Coastal Research, previously Marine and Coastal Management (MCM), who participated in the data collection and sample analysis. Data used in this study can be accessed via the South African Data Centre for Oceanography (SADCO) (http://sadco.csir.co.za/). Special thanks go to Marco Marcelino Worship for the role he played as Chief Scientist and for the coordination of the SHBML cruises between 2004 and 2011. DEA is further thanked for funding and facilities used.

## References

Andrews, W. R. H., and L. Hutchings (1980), Upwelling in the Southern Benguela Current, *Prog. Oceanogr.*, *9*, 1–81.

Atkinson, L. J., R. W. Leslie, J. G. Field, and A. Jarre (2011), Changes in demersal fish assemblages on the west coast of South Africa, 1986–2009, *Afr. J. Mar. Sci.*, *33*, 157–170.

Bailey, G. W., and P. Chapman (1985), The nutrient status of the St Helena Bay region in February 1979, in *South African Ocean Colour and Upwelling Experiment*, edited by L. V. Shannon, pp. 125–145, Sea Fish. Res. Inst., Cape Town.

Bang, N. D., and W. R. H. Andrews (1974), Direct current measurements of a shelf-edge frontal jet in the southern Benguela system, *J. Mar. Res.*, *32*, 405–417.

Barange, M., and S. Pillar (1992), Cross-shelf circulation, zonation and maintenance mechanisms of *Nyctiphanes capensis* and *Euphausia hanseni* (Euphausiacea) in the northern Benguela upwelling system, *Cont. Shelf Res.*, *12*, 1027–1042.

Bartholomae, C. H., and A. K. van der Plas (2007), Towards the development of environmental indices for the Namibian shelf, with particular reference to fisheries management, *Afr. J. Mar. Sci.*, *29*, 25–35.

Blamey, L. K., J. A. E. Howard, J. Agenbag, and A. Jarre (2012), Regime-shift detection in the southern Benguela, with particular reference to inshore ecosystems, *Prog. Oceanogr.*, *106*, 80–95.

Boyd, A. J., and G. Nelson (1998), Variability of the Benguela Current off the Cape Peninsula, South Africa, *S. Afr. J. Mar. Sci.*, *19*, 27–40.

Buys, M. E. L. (1957), Temperature variations in the upper 50 m in the St Helena Bay area, September 1950 to August 1957, *Invest. Rep. 27*, pp. 1–114, Div. of Sea Fish., Cape Town.

Buys, M. E. L. (1959), Hydrographical environment and the commercial catches 1950 to August 1957, *Invest. Rep. 37*, pp. 1–176, Div. of Sea Fish., Cape Town.

Carpenter, J. H. (1965), The Chesapeake Bay Institute technique for the Winkler dissolved oxygen method, *Limnol. Oceanogr.*, *10*, 141–143.

Carritt, D. E., and J. H. Carpenter (1966), Comparison and evaluation of currently employed modifications of the Winkler method for determining dissolved oxygen in seawater: A NASCO report, *J. Mar. Res.*, *24*, 286–318.

Chapman, P., and L. V. Shannon (1985), The Benguela ecosystem, Part 2. Chemistry and related processes, *Oceanogr. Mar. Biol. Ann. Rev.*, *23*, 183–251.

Cockcroft, A. C. (2001), Jasus Lalandii "walkouts" or mass strandings in South Africa during the 1990s: An overview, *Mar. Freshwater Res.*, *52*, 1085–1094.

Cockcroft, A. C., D. van Zyl, and L. Hutchings (2008), Large-scale changes in the spatial distribution of South African West Coast rock lobsters: An overview, *Afr. J. Mar. Sci.*, *30*, 149–159.

Crichton, M., L. Hutchings, T. Lamont, and A. Jarre (2013), From physics to phytoplankton: Prediction of dominant cell size in St Helena Bay in the Southern Benguela, *J. Plankton Res.*, *35*, 526–541.

Demarcq, H., R. G. Barlow, and L. Hutchings (2007), Application of a chlorophyll index derived from satellite data to investigate the variability of phytoplankton in the Benguela ecosystem, *Afr. J. Mar. Sci.*, *29*, 271–282.

Donners, J., S. S. Drijfhout, and W. Hazeleger (2005), Water mass transformations and subduction in the South Atlantic, *J. Phys. Oceanogr.*, *35*, 1841–1860.

Duncombe Rae, C. M. (2005), A demonstration of the hydrographic partition of the Benguela upwelling ecosystem at 26°40'S, *Afr. J. Mar. Sci.*, *27*, 617–628.

Duncombe Rae, C. M., A. J. Boyd, and R. J. M. Crawford (1992a), "Predation" of anchovy by an Agulhas ring: A possible contributory cause for the very poor year-class of 1989, *S. Afr. J. Mar. Sci.*, *12*, 167–173.

Duncombe Rae, C. M., F. A. Shillington, J. J. Agenbag, J. Taunton-Clark, and M. L. Gründlingh (1992b), An Agulhas ring in the South Atlantic Ocean and its interaction with the Benguela upwelling frontal system, *Deep Sea Res., Part A, 39*, 2009–2027.

Emery, W. J., and R. E. Thomson (2001), *Data Analysis Methods in Physical Oceanography*, 638 pp., Elsevier, Amsterdam.

Fairweather, T. P., M. Hara, C. D. van der Lingen, J. Raakjær, L. J. Shannon, G. G. Louw, P. Degnbol, and R. J. M. Crawford (2006), A knowledge base for management of the capital-intensive fishery for small pelagic fish off South Africa, *Afr. J. Mar. Sci.*, *28*, 645–660.

Garzoli, S. L., and A. L. Gordon (1996), Origins and variability of the Benguela Current, *J. Geophys. Res.*, *101*, 897–906.

Gordon, A. L. (1981), South Atlantic thermocline ventilation, *Deep Sea Res., Part A*, *28*, 1239–1264.

Hamukuaya, H., M. J. O'Toole, and P. M. Woodhead (1998), Observation of severe hypoxia and offshore displacement of Cape Hake over the Namibian shelf in 1994, *S. Afr. J. Mar. Sci.*, *19*, 57–59.
Hanawa, K., and L. D. Talley (2001), Mode waters, in *Ocean Circulation and Climate, Int. Geophys. Ser.*, edited by G. Siedler and J. Church, pp. 373–386, Academic, San Diego, Calif.
Hardman-Mountford, N. J., A. J. Richardson, J. J. Agenbag, E. Hagen, L. Nykjaer, F. A. Shillington, and C. Villacastin (2003), Ocean climate of the South East Atlantic observed from satellite data and wind models, *Prog. Oceanogr.*, *59*, 181–221.
Heywood, K. J., and B. A. King (2002), Water masses and baroclinic transports in the South Atlantic and Southern Oceans, *J. Mar. Res.*, *60*, 639–676.
Holden, C. (1987), Observations of low-frequency currents and continental shelf waves along the west coast of South Africa, *S. Afr. J. Mar. Sci.*, *5*, 197–208.
Huggett, J., H. Verheye, R. Escribano, and T. Fairweather (2009), Copepod biomass, size composition and production in the southern Benguela: Spatio-temporal patterns of variation, and comparison with other eastern boundary upwelling systems, *Prog. Oceanogr.*, *83*, 197–207.
Hutchings, L., M. R. Roberts, and H. M. Verheye (2009a), Marine environmental monitoring programmes in South Africa: A review, *S. Afr. J. Sci.*, *105*, 94–102.
Hutchings, L., et al. (2009b), The Benguela Current: An ecosystem in four components, *Prog. Oceanogr.*, *83*, 15–32.
Hutchings, L., A. Jarre, T. Lamont, M. van den Berg, and S. Kirkman (2012), St Helena Bay (southern Benguela) then and now: Muted climate signals, large human impact, *Afr. J. Mar. Sci.*, *34*, 559–583.
IOC, SCOR, and IAPSO (2010), The international thermodynamic equation of seawater—2010, Calculation and use of thermodynamic properties, in *Intergovernmental Oceanographic Commission Manuals and Guides* [in English], vol. 56, 196 pp., UNESCO. [Available at http://www.teos-10.org/pubs/TEOS-10_Manual.pdf.]
Jarre, A., L. Hutchings, M. Crichton, K. Wieland, T. Lamont, L. K. Blamey, C. Illert, E. Hill, and M. van den Berg (2015), Oxygen-depleted bottom waters along the west coast of South Africa, 1950–2011, *Fish. Oceanogr.*, *24*, suppl. 1, 56–73.
Jenkins, G. M., and D. G. Watts (1968), *Spectral Analysis and Its Applications*, 525 pp., Holden-Day, San Francisco, Calif.
Jury, M. R. (1985), Case studies of alongshore variations in wind-driven upwelling in the southern Benguela region, in *South African Ocean Colour and Upwelling Experiment*, edited by L. V. Shannon, pp. 29–46, Sea Fish. Res. Inst., Cape Town.
Kamstra, F. (1985), Environmental features of the southern Benguela with special reference to the wind stress, in *South African Ocean Colour and Upwelling Experiment*, edited by L. V. Shannon, pp. 13–27, Sea Fish. Res. Inst., Cape Town.
Kearns, E. J., and M.-E. Carr (2003), Seasonal climatologies of nutrients and hydrographic properties on quasi-neutral surfaces for four coastal upwelling systems, *Deep Sea Res., Part II*, *50*, 3171–3197.
Lett, C., C. Roy, A. Levasseur, C. van der Lingen, and C. Mullon (2006), Simulation and quantification of enrichment and retention processes in the southern Benguela upwelling ecosystem, *Fish. Oceanogr.*, *15*, 363–372.
Lett, C., J. Veitch, C. van der Lingen, and L. Hutchings (2007), Assessment of an environmental barrier to transport of ichthyoplankton from the southern to the northern Benguela ecosystem, *Mar. Ecol. Prog. Ser.*, *347*, 247–259.
Lutjeharms, J. R. E. (2006), *The Agulhas Current*, 329 pp., Springer, Berlin.
Lutjeharms, J. R. E., and J. M. Meeuwis (1987), The extent and variability of South-East Atlantic upwelling, *S. Afr. J. Mar. Sci.*, *5*, 51–62.
McCarthy, G., E. McDonagh, and B. King (2011), Decadal variability of thermocline and intermediate waters at 24°S in the South Atlantic, *J. Phys. Oceanogr.*, *41*, 157–165.
McCartney, M. S. (1982), The subtropical recirculation of mode waters, *J. Mar. Res.*, *40*, 427–464.
Monteiro, P. M. S., and A. N. Roychoudhury (2005), Spatial characteristics of sediment trace metals in an eastern boundary upwelling retention area (St Helena Bay, South Africa): A hydrodynamic-biological pump hypothesis, *Estuarine Coastal Shelf Sci.*, *65*, 123–134.
Monteiro, P. M. S., and A. K. van der Plas (2006), Low Oxygen Water (LOW) variability in the Benguela system: Key processes and forcing scales relevant to forecasting, in *Benguela: Predicting a Large Marine Ecosystem, Large Mar. Ecosyst. Ser.*, vol. 14, edited by V. Shannon et al., pp. 71–90, Elsevier, Amsterdam.
Monteiro, P. M. S., A. K. van der Plas, G. W. Bailey, and Q. Fidel (2004), Low oxygen variability in the Benguela ecosystem: A review and new understanding, *CSIR Rep. ENV-S-C 2004-075*, Stellenbosch, Council for Scientific and Industrial Research (CSIR), South Africa.
Monteiro, P. M. S., G. Nelson, A. van der Plas, E. Mabille, G. W. Bailey, and E. Klingelhoeffer (2005), Internal tide-shelf topography interactions as a forcing factor governing the large-scale distribution and burial fluxes of particulate organic matter (POM) in the Benguela upwelling system, *Cont. Shelf Res.*, *25*, 1864–1876.
Monteiro, P. M. S., et al. (2006), Low Oxygen Water (LOW) forcing scales amenable to forecasting in the Benguela ecosystem, in *Benguela: Predicting a Large Marine Ecosystem, Large Mar. Ecosyst. Ser.*, vol. 14, edited by V. Shannon et al., pp. 295–308, Elsevier, Amsterdam.
Monteiro, P. M. S., B. Dewitte, M. I. Scranton, A. Paulmier, and A. K. van der Plas (2011), The role of open ocean boundary forcing on seasonal to decadal-scale variability and long-term change of natural shelf hypoxia, *Environ. Res. Lett.*, *6*, 1–18, doi:10.1088/1748–9326/6/2/025002.
Nelson, G. (1985), Notes on the Physical Oceanography of the Cape Peninsula upwelling system, in *South African Ocean Colour and Upwelling Experiment*, edited by L. V. Shannon, pp. 63–95, Sea Fish. Res. Inst., Cape Town.
Nelson, G. (1989), Poleward motion in the Benguela area, in *Poleward Flows Along Eastern Ocean Boundaries, Coastal Estuarine Stud.*, vol. 34, edited by S. J. Neshyba et al., pp. 110–130, Springer, N. Y.
Nelson, G., and L. Hutchings (1983), The Benguela upwelling area, *Prog. Oceanogr.*, *12*, 333–356.
Nelson, G., and A. Polito (1987), Information on currents in the Cape Peninsula area, South Africa, *S. Afr. J. Mar. Sci.*, *5*, 287–304.
Núñez-Riboni, I., O. Boebel, M. Ollitrault, Y. You, P. L. Richardson, and R. Davis (2005), Lagrangian circulation of Antarctic Intermediate Water in the subtropical South Atlantic, *Deep-Sea Res. II*, *52*, 545–564.
Payne, A. I. L., and A. E. Punt (1995), Biology and Fisheries of South African Cape hakes (*M. capensis* and *M. paradoxus*), in *Hake, Biology and Markets*, edited by J. Alheit and T. J. Pitcher, pp. 15–47, Chapman and Hall, London, U. K.
Penven, P., C. Roy, A. Colin de Verdière, and J. Largier (2000), Simulation of a coastal jet retention process using a barotropic model, *Oceanol. Acta*, *23*, 615–634.
Pitcher, G. C., and G. Nelson (2006), Characteristics of the surface boundary layer important to the development of red tide on the southern Namaqua shelf of the Benguela upwelling system, *Limnol. Oceanogr.*, *51*, 2660–2674.
Pitcher, G. C., and T. A. Probyn (2011), Anoxia in southern Benguela during the autumn of 2009 and its linkage to a bloom of the dinoflagellate *Ceratium balechii*, *Harmful Algae*, *11*, 23–32.

Pitcher, G. C., T. A. Probyn, A. du Randt, A. J. Lucas, S. Bernard, H. Evers-King, T. Lamont, and L. Hutchings (2014), Dynamics of oxygen depletion in the nearshore of a coastal embayment of the southern Benguela upwelling system, *J. Geophys. Res. Oceans*, *119*, 2183–2200, doi: 10.1002/2013JC009443.

Provost, C., C. Escoffier, K. Maamatuaiahutapu, A. Kartavtseff, and V. Garçon (1999), Subtropical mode waters in the South Atlantic, *J. Geophys. Res.*, *104*, 21,033–21,049.

Sallée, J.-B., K. Speer, S. Rintoul, and S. Wijffels (2010), Southern ocean thermocline ventilation, *J. Phys. Oceanogr.*, *40*, 509–529.

Sato, O. T., and P. S. Polito (2014), Observation of South Atlantic subtropical mode waters with Argo profiling float data, *J. Geophys. Res. Oceans*, *119*, 2860–2881, doi:10.1002/2013JC009438.

Shannon, L. V. (1985), The Benguela ecosystem, Part 1. Evolution of the Benguela, physical features and processes, *Oceanogr. Mar. Biol. Ann. Rev.*, *23*, 105–182.

Shannon, L. V., and J. J. Agenbag (1990), A large-scale perspective on interannual variability in the environment in the South-East Atlantic, *S. Afr. J. Mar. Sci.*, *9*, 161–168.

Shannon, L. V., and G. Nelson (1996), The Benguela: Large scale features and processes and system variability, in *The South Atlantic: Present and Past Circulation*, edited by G. Wefer et al., pp. 163–210, Springer, Berlin.

Shannon, L. V., L. Hutchings, G. W. Bailey, and P. A. Shelton (1984), Spatial and temporal distribution of chlorophyll in southern African waters as deduced from ship and satellite measurements and their implications for pelagic fisheries, *S. Afr. J. Mar. Sci.*, *2*, 109–130.

Shannon, L. V., J. R. E. Lutjeharms, and J. J. Agenbag (1989), Episodic input of Subantarctic water into the Benguela region, *S. Afr. J. Sci.*, *85*, 317–322.

Shannon, L. V., J. J. Agenbag, N. D. Walker, and J. R. E. Lutjeharms (1990), A major perturbation in the Agulhas retroflection area in 1986, *Deep Sea Res., Part A*, *37*, 493–512.

Shannon, L. V., G. Hempel, P. Malanotte-Rizzoli, C. L. Moloney, and J. Woods (2006), *Benguela: Predicting a Large Marine Ecosystem, Large Mar. Ecosyst.* [CD-ROM], vol. 14, 410 pp., Elsevier, Amsterdam.

Shelton, P. A., and L. Hutchings (1990), Ocean stability and anchovy spawning in the southern Benguela Current region, *Fish. Bull.*, *88*, 323–338.

Shillington, F. A., C. J. C. Reason, C. M. Duncombe Rae, P. Florenchie, and P. Penven (2006), Large scale physical variability of the Benguela Current Large Marine Ecosystem (BCLME), in *Benguela: Predicting a Large Marine Ecosystem, Large Mar. Ecosyst.*, vol. 14, edited by V. Shannon et al., pp. 49–70, Elsevier, Amsterdam.

Stramma, L., and M. England (1999), On the water masses and mean circulation of the South Atlantic Ocean, *J. Geophys. Res.*, *104*, 20,863–20,883.

Taunton-Clark, J. (1985), The formation, growth and decay of upwelling tongues in response to the mesoscale wind field during summer, in *South African Ocean Colour and Upwelling Experiment*, edited by L. V. Shannon, pp. 47–61, Sea Fish. Res. Inst., Cape Town.

Tomczak, M., and J. S. Godfrey (2003), *Regional Oceanography: An Introduction*, 2nd ed., 390 pp., Daya Publ. House, Delhi, India.

Touratier, F., J. G. Field, and C. L. Moloney (2003), Simulated carbon and nitrogen flows of the planktonic food web during an upwelling relaxation period in St Helena Bay (southern Benguela ecosystem), *Prog. Oceanogr.*, *58*, 1–41.

van der Lingen, C. D., L. J. Shannon, P. Cury, A. Kreiner, C. L. Moloney, J.-P. Roux, and F. Vaz-Velho (2006), Resource and ecosystem variability, including regime shifts, in the Benguela Current System, in *Benguela: Predicting a Large Marine Ecosystem, Large Mar. Ecosyst.*, vol. 14, edited by V. Shannon et al., pp. 147–185, Elsevier, Amsterdam.

Veitch, J., P. Penven, and F. Shillington (2009), The Benguela: A laboratory for comparative modelling studies, *Prog. Oceanogr.*, *83*, 296–302.

Veitch, J., P. Penven, and F. Shillington (2010), Modeling equilibrium dynamics of the Benguela Current system, *J. Phys. Oceanogr.*, *40*, 1942–1964.

Weeks, S. J., R. Barlow, C. Roy, and F. A. Shillington (2006), Remotely sensed variability of temperature and chlorophyll in the southern Benguela: Upwelling frequency and phytoplankton response, *Afr. J. Mar. Sci.*, *28*, 493–509.

You, Y. (2002), Quantitative estimate of Antarctic Intermediate Water contributions from the Drake Passage and the southwest Indian Ocean to the South Atlantic, *J. Geophys. Res.*, *107*(C2), 3031, doi:10.1029/2001JC000880.